Analysis and Design of Retrodirective Arrays for Multiple-Interrogator Environments

A THESIS SUBMITTED TO THE GRADUATE DIVISION OF THE UNIVERSITY OF HAWAIʻI IN PARTIAL FULFILLMENT OF THE REQUIREMENTS FOR THE DEGREE OF

MASTER OF SCIENCE

IN

ELECTRICAL ENGINEERING

December 2010

By
Tyler F. Chun

Thesis Committee:

Wayne A. Shiroma, Chairperson
Aaron T. Ohta
Zhengqing Yun

We certify that we have read this thesis and that, in our opinion, it is satisfactory in scope and quality as a thesis for the degree of Master of Science in Electrical Engineering.

THESIS COMMITTEE

_____

Chairperson

_____

_____

Analysis and Design of Retrodirective Arrays for Multiple-Interrogator Environments

by

Tyler F. Chun

To my mom, dad, and brothers Ryan and Kasey. Thank you for all your love and support. I couldn't have done it without you guys!

Acknowledgments

First, I would like to thank my advisor Dr. Wayne Shiroma for providing me with this tremendous opportunity. Through the mentorship of Dr. Shiroma I have grown not only academically, but also as a person.

I would also like to thank Dr. Zhengqing Yun and Dr. Aaron Ohta, for their willingness to serve on my thesis defense committee and for the valuable advice and support they have given me throughout my career as a graduate student.

To the past and present members of the MMRL group: Brandon Takase, Ryan Pang, Justin Akagi, Monte Watanabe, Alex Zamora, Reece Iwami, Toy Lim, Wade Tonaki, Bao Jun Lei, and Joseph Longhi, it has been a pleasure getting to know all of you. I'll miss you guys.

Finally, I would like to thank the National Consortium for MASINT Research for funding my research.

Abstract

Retrodirective arrays are an attractive technology for mobile, wireless devices because of their capability to autonomous steer a beam. This thesis focuses on the analysis and design of retrodirective-array technology for multiple-interrogator environments. A performance assessment of the phase-conjugating retrodirective array architecture in the presence of multiple interrogators is performed, showing that the phase-conjugating retrodirective array can retrordirect toward multiple interrogators. A retrodirective array architecture that uses interleaved retrodirective sub-arrays is presented. This interleaved retrodirective array is able to retrodirect its beam toward a single interrogator, while steering a null in a different direction, which can be used for interference rejection.

Contents

List of Figures **v**

1 Introduction **1**
1.1 Antenna Background 1
1.2 Phased Arrays 4
1.2.1 Retrodirective Arrays 5
1.2.2 Phased Array Radiation Pattern 6
1.2.3 Radar Cross Section Measurements 8
1.3 Retrodirective Array Architectures 10

2 Analysis of Phase-Conjugating Arrays in the Presence of Multiple Interrogators **17**
2.1 Introduction 17
2.2 Theoretical Analysis 19
2.2.1 Single Interrogator Case 21
2.2.2 Double Interrogator Case 22
2.3 Experimental Verification 27
2.3.1 Array Characteristics 27
2.3.2 Effects of Phase Difference Between Interrogators 28
2.3.3 Effect of Interrogator Incident Angle 30

3 An Interleaved Inter-Element Phase-Detecting, Phase-Shifting Retrodirective Array for Interference Rejection **34**
3.1 Introduction 34
3.2 Design 38
3.2.1 Retrodirective Sub-Array 42
3.2.2 Null Steering 51
3.3 Experimental Results 52
3.4 Conclusions 56

4 Conclusions and Future Work **57**
4.1 Conclusions 57

4.2 A Beam-Scanning Liquid-Metal Reflectarray 59
4.3 Interference Identification and Null-Forming Circuitry 62

Bibliography **63**

List of Figures

1.1 Mechanically steered dish antenna systems. 3
1.2 Geometry for phased array calculations using a two-element array. 4
1.3 Standard setup used to measure the radiation pattern of an antenna. 7
1.4 Geometry for phased array calculations using a two-element array. 11
1.5 Pon array schematic. 12
1.6 Schematic of the phase-detecting/phase-shifting RDA architecture. 13
1.7 Transmit array for the phase-detecting/heterodyne-scanning RDA from [7] . 14
1.8 Schematic of the power-detecting/phase-shifting RDA architecture from [8]. 16

2.1 Multiple interrogator situations. (a) Multi-user network, (b) multipath environment 18
2.2 Geometry used in theoretical analysis. 19
2.3 Electric field, E_{Tx}, due to a single interrogator at $\theta = 20^\circ$ 21
2.4 Predicted RCS for a (a) four-element and (b) eight-element PCA in response to a single interrogator at $\theta = 20^\circ$ 22
2.5 Normalized transmitted electric field for (a) in-phase (b) out-of-phase interrogators at $\pm 20^\circ$. The x-axis is in units of quarter wavelengths. The circles denotes the electric field at each element of a four-element array, and the asterisks represent the eight-element case. 23
2.6 Predicted multistatic RCS as a function of phase difference between interrogators with $\theta = \pm 20^\circ$ on (a) a four-element PCA and (b) an eight-element array. 24
2.7 (a) Monostatic RCS and (b) bistatic RCS with interrogator at 20° for the four-element PCA. 26
2.8 (a) Monostatic RCS and (b) bistatic RCS with interrogator at 20° for the eight-element PCA. 26
2.9 General experimental setup. 28
2.10 Far-field multistatic RCS for a four-element PCA interrogated by (a) two out-of-phase sources with $\theta = \pm 20^\circ$, (b) two in-phase sources with $\theta = \pm 20^\circ$. 29
2.11 Far-field multistatic RCS for a eight-element PCA interrogated by (a) two out-of-phase sources with $\theta = \pm 20^\circ$, (b) two in-phase sources with $\theta = \pm 20^\circ$. 30
2.12 Effect of phase difference between interrogators on transmitted electric field. 31

2.13 Far-field multistatic RCS for a four-element PCA interrogated by (a) two out-of-phase sources with $\theta = \pm 10°$, (b) two in-phase sources with $\theta = \pm 10°$. 31
2.14 Far-field multistatic RCS for a eight-element PCA interrogated by (a) two out-of-phase sources with $\theta = \pm 10°$, (b) two in-phase sources with $\theta = \pm 10°$. 32
2.15 Effect of incident angle on transmitted electric field. 33
2.16 Multistatic RCS of an eight-element PCA interrogated by two in-phase sources located at $-40°$ and $10°$. 33

3.1 A mobile phone user in the presence of an interferer. 36
3.2 A vehicle communicating with an aircraft in the presence of an eavesdropper. 37
3.3 Geometry for null-steering calculations 39
3.4 Schematic of the interleaved inter-element phase-detecting, phase-shifting retrodirective array for interference rejection. 40
3.5 Simulated RDA "element" pattern, array factor, and total radiation pattern for an interleaved RDA with interrogators located at $-30°$ and $0°$, and null steered to $-30°$. 42
3.6 Block diagram of the four-element retrodirective array using interelement phase detection and phase shifting from [6]. 43
3.7 Schematic of the patch antenna array. 44
3.8 Photograph of the final fabricated array. 45
3.9 Schematic of the phase-shifting array and phase detecting blocks from [6]. . 46
3.10 Phase shifter characteristic curve. 47
3.11 Comparator circuit to implement phase wrapping 47
3.12 Theoretical voltage versus phase difference curves for the two phase detectors in a phase-detecting block. 49
3.13 Detailed schematic of the phase detecting block between elements 1 and 2, showing the implementation of the two phase detectors and comparator to achieve a $360°$ detection range. 50
3.14 Layout of the power divider with phase delay. 52
3.15 Picture of a complete retrodirective sub-array (without antenna array) . . . 53
3.16 Bistatic RCS for sub-array 1 with Bistatic RCS for sub-array 2 with interrogators at (a) $0°$ and (b) $-20°$. 54
3.17 Multistatic RCS of the interleaved array with interrogators at $\pm 30°$ (a) with no null formed, (b) with null steered to $30°$, and (c) with null steered to $-30°$. 55

4.1 (a) A typical reflectarray using microstrip patch antenna elements with open-circuit stubs (b) Liquid metal reflectarray using EGaIn on a electrode grid. 60

Chapter 1

Introduction

1.1 Antenna Background

Consider the conceptually simplest type of radiator, an isotropic antenna, which radiates equally in all directions. This source creates a spherical wave, which has an electric field with uniform amplitude and phase over any spherical surface so long as the isotropic antenna is located at the center of that sphere. As the wave from this antenna propagates, the power spreads over a progressively larger sphere. The power density at distance R from the antenna is simply the input power of the antenna divided by the surface area of a sphere with radius R:

$$W_0 = \frac{P_{in}}{4\pi R^2}. \tag{1.1}$$

Another way to express the radiation characteristics of an antenna is the radiation intensity, which describes the power radiated per unit solid angle. The radiation intensity of an

isotropic antenna is the input power divided by the solid angle of a sphere,

$$U_0 = \frac{P_{in}}{4\pi}. \tag{1.2}$$

However, an isotropic antenna is a theoretical creation; there is no known antenna that radiates equally in all directions. To characterize how well an antenna radiates in a given direction the concept of directivity is used. The directivity is the ratio of the radiation intensity of the antenna under test (AUT) to the radiation intensity of the isotropic antenna,

$$D(\theta, \phi) = \frac{U(\theta, \phi)}{U_0}. \tag{1.3}$$

Directivity is usually expressed using a logarithmic scale [dBi]. Some antenna manufacturers use a dipole antenna to characterize their AUT, so the directivity provided is the ratio of the AUT's radiation intensity to that of a dipole antenna rather than that of an isotropic antenna. This measurement has units of [dBd].

The graph of the directivity versus angle, called the radiation pattern, represents the power radiated by the antenna versus angle, usually normalized to the maximum power and is one of the main measurements that characterizes an antenna. Through the reciprocal nature of antennas, the transmit pattern of the antenna is also the same as the receive pattern. So an antenna that directs most of its radiation in a particular direction also collects most of its received signal from that direction.

Most antennas have a fixed radiation pattern, however there are several ways that one can achieve beam steering. This first is to mount a directional antenna on a mechanically steered platform. Beam steering is accomplished by physically moving the antenna

Figure 1.1: Mechanically steered dish antenna systems.

therefore changing the radiation pattern of the system. Fig. 1.1 shows a mechanically steered parabolic dish antenna. This type of system can achieve high directivity but the mechanical nature of the system leads to reliability issues as well as limits the rate at which the beam can be steered.

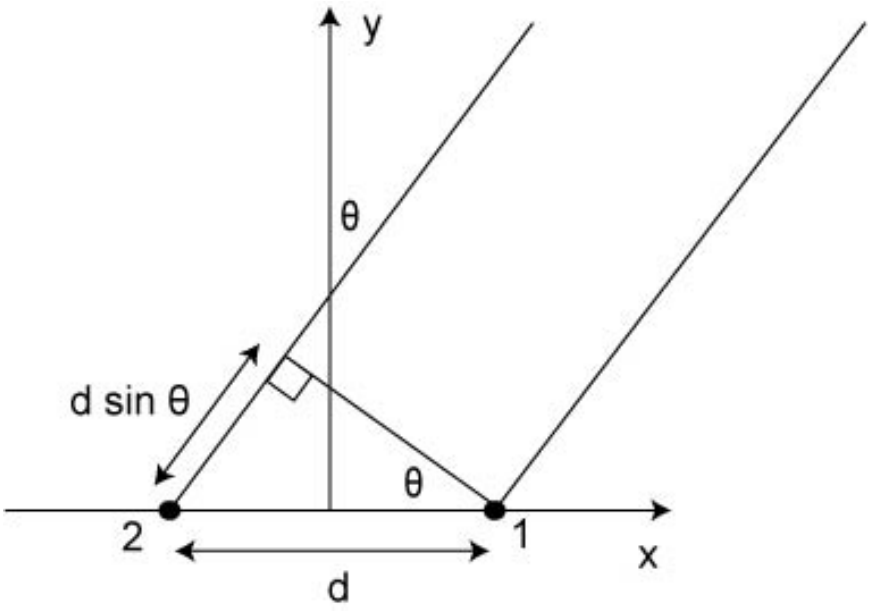

Figure 1.2: Geometry for phased array calculations using a two-element array.

1.2 Phased Arrays

Another way to steer a beam is electronically by using a phased array. A phased array is composed of multiple antennas, individually called elements, fed with the same signal but with a slightly different phase, so that the radiation from the antenna elements constructively interfere in the desired direction. All array elements are fed from the same source, with the phase to each element typically controlled using phase shifters placed at each element.

Consider the two-element array of isotropic antennas, with an element spacing of d, shown in Fig. 1.2. For a plane wave incident from angle θ, the path length from the source, to element 2, is $d \sin\theta$ longer than the path length from the source to element 1. This means that the phase at element 2 will be $kd \sin\theta$ less than the phase at element 1 due

to the extra phase delay incurred, where k is the wavenumber. The relationship between the phase difference between elements and the angle of the main beam for a phased array is given by

$$\phi = kd\sin\theta, \tag{1.4}$$

where ϕ is the phase difference between elements, and $k = 2\pi/\lambda$. For communications systems using typical phased arrays, it is necessary to know the locations of both the phased array, and target node so that the angle θ can be determined

1.2.1 Retrodirective Arrays

A retrodirective antenna (RDA) is a type of phased array that is able to sense the direction of an incoming interrogating signal and send a reply in that same direction [1]. To understand how an RDA works, consider again the example in Fig. 1.2. If the two-element array is now transmitting in the direction of θ rather than receiving, there is still the extra path length ($d\sin\theta$) from element 2 to the source compared to that from element 1 to the source. But now since the direction of propagation is reversed (i.e., $\vec{k}$ is reversed), the phase delay due to propagation is also reversed, and the phase at element 1 must be $kd\sin\theta$ less than that at element 2. So to convert from an incident wave at angle θ to an outgoing wave at angle θ, the phase difference between elements must be reversed. This is the condition needed to achieve retrodirectivity.

Note that phase conjugating, or negating the phase, at each element has the effect of reversing the phase difference between each pair of antenna elements so phase conjugation

also facilitates retrodirectivity. Through the relationship between the frequency domain and time domain, it can also be shown that a phase conjugation in the frequency domain corresponds to a time reversal in the time domain,

$$F(-j\omega) \rightarrow f(-t). \tag{1.5}$$

Time-reversed acoustics operates on sound waves in the time domain to retrodirect them back to their source [2]. The different RDA architectures are described later in this chapter.

1.2.2 Phased Array Radiation Pattern

The radiation pattern of phased arrays is calculated in a method similar to that of a single antenna but now the radiation pattern of each element contributes to the total radiation pattern of the array. The law of superposition is used to determine the radiation pattern created by the two-element system of Fig. 1.2.

With the phase of element 1 as the reference, the total electric field E is given by

$$E(\theta) = 1 + e^{-j(kd\sin\theta+\phi)}, \tag{1.6}$$

where $k = 2\pi/\lambda$, d is the element spacing, ϕ is the phase difference between elements, and θ is the angle at which the electric field calculation is desired (not the angle of incidence of the plane wave). This result can be extended to an N-element array of isotropic elements with uniform amplitude and spacing (d) to be

$$AF(\theta) = \sum_{n=1}^{N} e^{-j(n-1)\psi}, \tag{1.7}$$

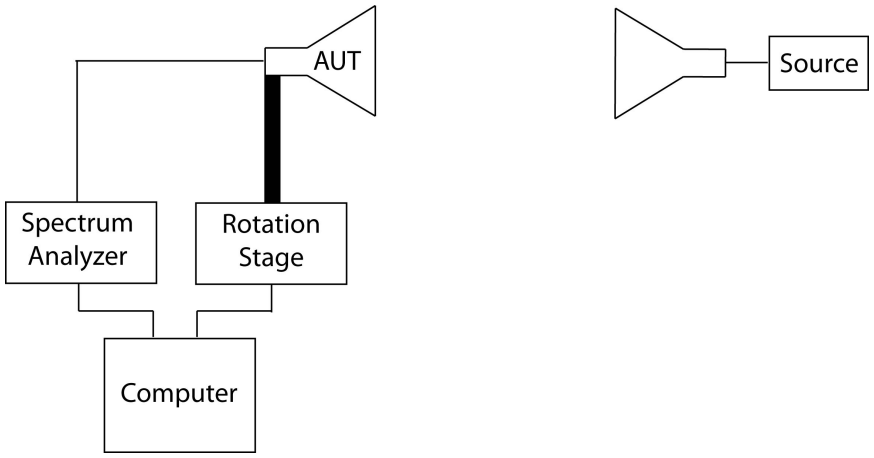

Figure 1.3: Standard setup used to measure the radiation pattern of an antenna.

where $\psi = kd\sin\theta + \phi$.

Note that all the previous derivations were performed under the assumption of array elements being isotropic sources. For arrays using other types of antennas as the array element, the total radiation pattern is obtained by multiplying the pattern for the array using isotropic elements (known as the array factor AF) by the individual pattern of the antenna element used in the array:

$$E_{total}(\theta) = AF \times \text{element pattern.} \tag{1.8}$$

The actual radiation pattern measurement is usually performed on an antenna range or in an anechoic chamber. The AUT is placed on a rotation stage with a fixed horn antenna facing the AUT placed in the far field. The horn antenna is fed an RF signal from an RF source and the AUT is attached to a spectrum analyzer. As the AUT is rotated by the rotation stage, the power received and the angle is recorded and plotted. Fig. 1.3 shows a typical setup.

1.2.3 Radar Cross Section Measurements

Because of the nature of RDAs, the setup typically used to measure the radiation pattern of phased array antennas (Fig. 1.3) cannot be used to measure the radiation pattern of the RDA. For proper RDA operation, there must be an interrogating signal that the RDA can then respond to with a retrodirected signal. This behavior of sending a signal (interrogation) then receiving a signal back (retrodirection) is similar to an illumination and resulting reflections seen in the realm of radar measurements. As a result, the setup used to take RDA measurements are more akin to the setups used to measure radar cross section (RCS) than normal antenna radiation patterns.

In radar systems, a signal transmitted by the radar propagates through space until it reaches the target. Some power from the signal is reflected back in the direction of the radar, resulting in some received power, P_r back at the radar. The RCS (σ) of a target gives some indication as to the size that a target looks to the radar, measured in [m^2]. Consider a radar system operating on a target. The radar range equation is

$$P_r = \frac{P_t G_t}{4\pi r^2} \sigma \frac{1}{4\pi r^2} A_{eff}. \tag{1.9}$$

where P_t is the transmit power, G_t is the gain of the transmit antenna, r is the distance between the radar system and the target, and A_{eff} is the effective area of the receive antenna. Analyzing the right side of (1.9), the term $P_t G_t/(4\pi r^2)$ represents the power density at the target. So $\sigma P_t G_t/(4\pi r^2)$ is the power "captured" by the target. The $1/(4\pi r^2)$ is the isotropic spreading factor of a signal as it propagates through space. The power "captured" multiplied by the spreading factor yields a power density, which when multiplied by the effective area of the antenna, A_{eff}, results in the received power back at the radar.

So the RCS is technically the surface area required at the target to collect the necessary power, $P_{iso} = \sigma P_t G_t/(4\pi r^2)$, such that if P_{iso} were radiated by an isotropic source (at the location of the target) the power received by the radar receiver would match the power received from the signal's reflection off the target P_r.

There are two types of RCS measurements that must be considered: the monostatic RCS and the bistatic RCS. In monostatic radar, the receiver and transmitter are co-located and the angle between the radar and the target are varied. For RDA measurements the monostatic RCS setup demonstrates that the RDA can track a moving target. The RDA should always point toward the interrogator and since the co-located interrogator/receiver pair is swept across the RDA's field of view, the power level should remain constant with angle.

In the second type of RCS measurement, the bistatic RCS, the transmitter and receiver are not co-located, the transmitter remains fixed, while the receiver is swept in angle with respect to the target. In this measurement set up the interrogator's angle with respect to the RDA is constant, and the swept receiving horn measures the radiation pattern created by the RDA. A variation of the bistatic RCS is the multistatic RCS in which there are multiple transmitters. Throughout this thesis, the RDA measurements are referred to by the type of measurement setup that was used (i.e., monostatic RCS or bistatic RCS). This is done to differentiate between the two types of measurements, but the RCS of the RDAs are not actually measured.

1.3 Retrodirective Array Architectures

Retrodirective arrays are by no means a new technology. Since the first RDA was created in 1960, numerous RDA architectures have been developed. This section describes the most common RDA architectures and discusses their strengths and drawbacks.

Van Atta Array

The Van Atta array [3] is the simplest type of RDA. Fig. 1.4 shows a schematic of a four-element Van Atta array. For this array, pairs of corresponding elements, in this case, elements one and four; and elements two and three, are connected with equal length transmission lines. As the signal is received at each element it propagates down the transmission line and radiates from the corresponding element. So, if the incoming wave creates a uniform phase gradient across the array, i.e., is a plane wave, that phase gradient across the array is reversed for the transmitted wave.

However, there are some disadvantages to this array. The Van Atta array only works for a single, plane-wave interrogator. The simplicity of this design makes it hard to connect to a transceiver making modulation and demodulation of data difficult. Also, since the input to one element becomes the output of another element the input and output signals are coupled. As the interrogating signal travels toward the source it incurs a loss in signal power proportional to R^2. Since the output signal power is dependent on the input signal power, this R^2 path loss is propagated to the outgoing wave, which then incurs another R^2 path loss on the return trip, for a total roundtrip path loss proportional to R^4.

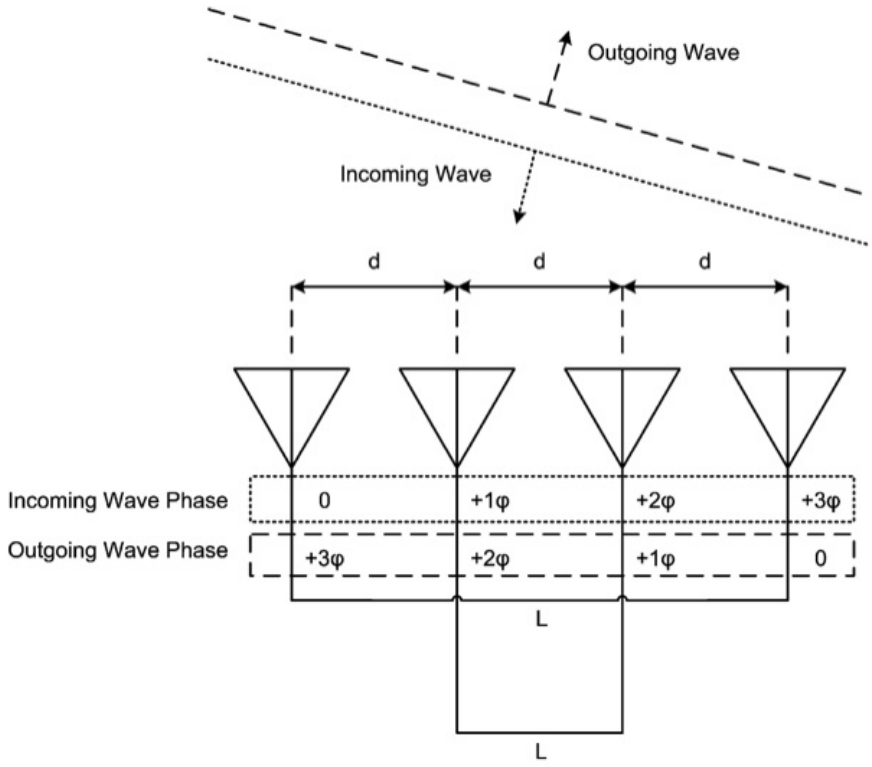

Figure 1.4: Geometry for phased array calculations using a two-element array.

Pon Array

The Pon array, or heterodyne phase-conjugating RDA, is one of the most common types of RDAs, first presented by Pon in 1964 [4]. Fig. 1.5 shows a schematic of the heterodyne phase-conjugating array. This type of array uses mixers to achieve phase conjugation. Mixers carry out the operation

$$\begin{aligned} V_O &= \cos(\omega_{LO}t)\cos(\omega_{RF}t+\phi) \\ &= \frac{1}{2}\left(\cos((\omega_{LO}-\omega_{RF})t-\phi)\cos((\omega_{LO}+\omega_{RF})t+\phi)\right). \end{aligned}$$

If the local oscillator (LO) frequency is set to $2\omega_{RF}$ and the upper sideband is

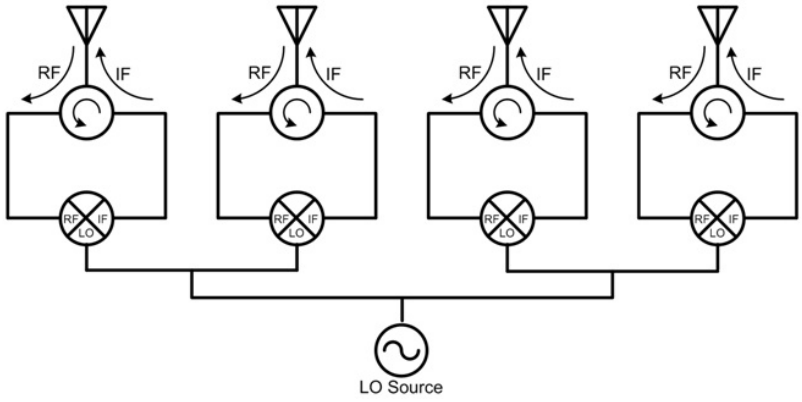

Figure 1.5: Pon array schematic.

filtered out, the resulting signal is simply the phase-conjugated version of the RF signal $(1/2\cos(\omega_{RF} - \phi))$. Since phase conjugating each element results in reversing the phase difference between elements, this architecture will retrodirect. The heterodyne phase-conjugating architecture is relatively simple and inexpensive to implement, since it only requires mixers and an LO, which is why this architecture is frequently used.

However, the heterodyne phase-conjugating array suffers from an R^4 path loss due to the dependence of the output signal on the input signal. On top of that, due to the mixing products, half of the original power goes to the unusable upper side band, resulting in a 3-dB loss in power. A performance analysis on the ability of the heterodyne phase-conjugating array to respond to multiple interrogators is presented in the next chapter.

Phase-Detecting/Phase-Shifting RDA

The phase-detecting/phase-shifting RDA [5] is shown in Fig. 1.6. This RDA consists of two different arrays, the two-element phase-detecting array and the transmitting

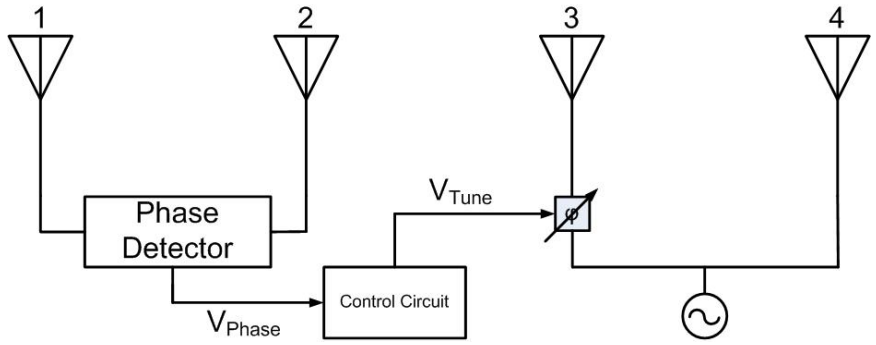

Figure 1.6: Schematic of the phase-detecting/phase-shifting RDA architecture.

array. A phase detector placed between the elements of the phase-detecting array determines the angle of arrival (AOA) of the incoming signal. An analog control circuit automatically adjusts the control voltages to the phase shifters in the transmitting array to properly phase the transmit array to respond back toward the interrogator. The phase shifters also facilitate the coherent combination of the received signal.

Compared with the other two RDAs, the phase-detecting/phase-shifting RDA only incurs an R^2 path loss because the output signal power is not dependent on the input signal power. Unlike the previous RDA, this RDA can only respond to a single, plane-wave source and cannot respond to multiple interrogators. The phase difference between each pair of elements is not reversed; instead a constant phase gradient is setup across the array allowing only a single beam to be steered. However, a later iteration of this architecture presented in [6] and described in depth in Chapter 3 remedies this shortcoming, enabling the array to retrodirect to multiple interrogators.

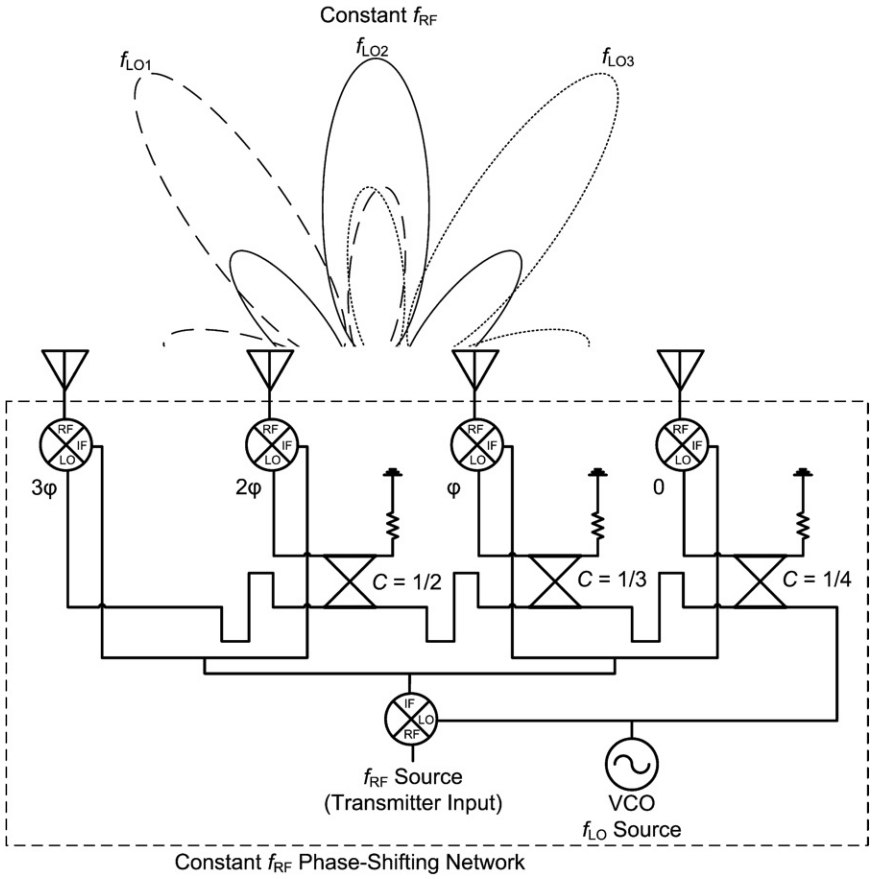

Figure 1.7: Transmit array for the phase-detecting/heterodyne-scanning RDA from [7]

Phase-Detecting/Heterodyne-Scanning RDA

The phase-detecting/heterodyne-scanning RDA [7] operates in a similar fashion to the phase-detecting/phase-shifting RDA. There are still two arrays, the phase-detecting array and the transmitting array, however instead of using a phase shifter in the transmit array to create the proper phasing, this architecture's transmit array uses heterodyne mixing in combination with frequency scanning for proper phasing. The phase-shifting portion of this array is shown in Fig. 1.7. In this architecture, the analog control circuit outputs a control voltage that controls the voltage-controlled oscillator (VCO) to steer the beam.

The electrical length of a delay line changes as the frequency of signal changes even though the physical length of delay line remains unchanged. By using a VCO to vary the frequency of the signal, the phase delay caused by the delay line can be varied. Mixers placed at each element mix an LO with the outgoing signal to ensure that the frequency of operation of the RDA remains constant. This architecture suffers from the same drawbacks as the phase-detecting/phase-shifting RDA architecture in that it cannot respond to multiple interrogators. Because the input and output signals are decoupled, this architecture only incurs an R^2 path loss.

Power-Detecting/Phase-Shifting RDA

The power-detecting/phase-shifting RDA [8] uses a concept entirely different from that used for the architectures that rely on phase detection to determine the AOA. In the power-detecting/phase-shifting architecture, the AOA of the interrogator is determined by power level. The array first steers a beam from -90° to 90° recording the power received at each angle. The angle with the highest received power is the angle that corresponds to the interrogator's direction. Fig. 1.8 shows a schematic of the power-detecting/phase-shifting RDA.

This RDA architecture has the advantage of being simple and can be made to fit within a small form factor. However, this RDA is not a full-duplex system as it must switch between a scanning mode to acquire the AOA of the interrogator, and a communication mode to transmit and receive data from the interrogating source. This RDA is also not capable of transmitting to multiple interrogators.

In most applications, RDAs operate in environments with multiple incident inter-

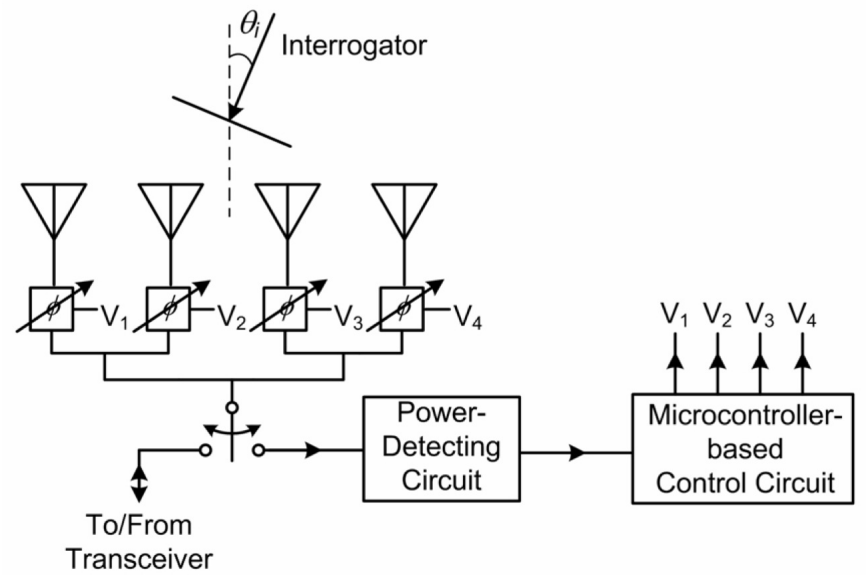

Figure 1.8: Schematic of the power-detecting/phase-shifting RDA architecture from [8].

rogating signals, whether it be due to multipath reflections, interferers, or multiple intended targets. The following chapter examines the performance of the phase-conjugating RDA architecture in the presence of multiple interrogating signals. Later, in Chapter 3, an architecture capable of interference rejection is presented.

Chapter 2

Analysis of Phase-Conjugating Arrays in the Presence of Multiple Interrogators

2.1 Introduction

Numerous applications exist in which an RDA might be interrogated by multiple sources and where a response to each interrogator is desired. An example is a mobile wireless network, multiple mobile nodes are in communication with a cell tower that contains an RDA front end (Fig. 2.1(a)). For optimum communication between cell tower and the multiple nodes, it is desired that the RDA front end direct its beams toward the multiple, interrogating sources.

Another example of an RDA operating under multiple-interrogator conditions oc-

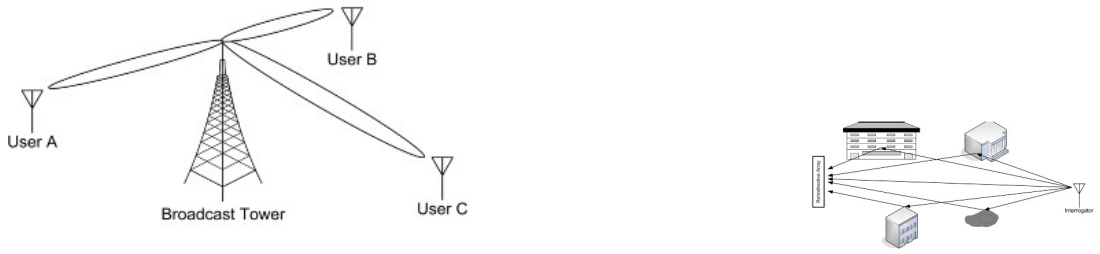

(a) (b)

Figure 2.1: Multiple interrogator situations. (a) Multi-user network, (b) multipath environment

curs in a multipath environment, where each reflected signal can be interpreted as a separate interrogator (Fig. 2.1(b)). Conventional omnidirectional antennas in multipath environments experience a fading effect due to the out-of-phase arrival of the various reflected signals at the antenna. RDAs have been shown to work in multipath environments, mitigating the multipath fading effect seen in conventional omnidirectional antennas [9] - [13], however there has been little work showing how variation in the interrogators' properties affects the RDA's performance.

Several RDA architectures utilizing phase-detecting and phase-shifting elements [6], and power-detecting and phase-shifting elements [8] have exhibited the ability to resolve and respond to multiple interrogators with varying levels of success. This chapter presents in full, the work partially described in [14] and [15] on the performance of phase-conjugating arrays (PCAs) in a multiple-interrogator environment.

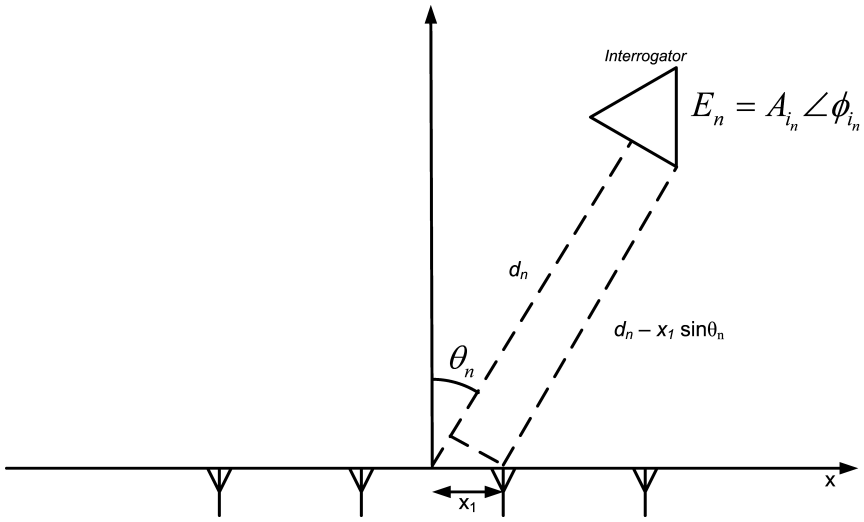

Figure 2.2: Geometry used in theoretical analysis.

2.2 Theoretical Analysis

A theoretical analysis of a PCA in the presence of multiple interrogators is performed; this analysis is later compared with experimental results to verify its merit. The simplest way to tackle this analysis is to begin with the simplest possible case, a PCA in the presence of a single interrogator.

Fig. 2.2 shows the geometry used for all analyses performed. The PCA defines the x-axis, where the center of the array is set to coincide with location $x = 0$. The angle between the interrogator and the array normal is defined as θ and is used along with the distance d to define the interrogator's location. For a single interrogator, the received electric field at any point along the x-axis is given by

$$\begin{aligned} E_{Rx} &= A_i e^{j\phi_i} e^{jkx\sin(\theta)} e^{-jkd} \\ &= A_i e^{j\phi} e^{jkx\sin\theta}, \end{aligned} \tag{2.1}$$

where $k = 2\pi/\lambda$ and the phase of the interrogating source and the phase delay due to propagation are lumped into $\phi = \phi_i - kd$, which represents the phase of the electric field from the interrogator at the center of the array ($x = 0$).

The signal received at x given by (2.1) will be phase conjugated and result in an electric field

$$E_{Tx} = A_i e^{-j\phi} e^{-jkx\sin\theta}. \tag{2.2}$$

To find the electric field at a particular element, one must substitute the appropriate value for x in (2.2). For example, a four-element array with uniform $\lambda/2$ spacing will have elements at $x = -3\lambda/4$, $-\lambda/4$, $\lambda/4$, and $3\lambda/4$.

The results of (2.1) and (2.2) can be extended to account for N interrogators using the principle of superposition. Each interrogator will contribute to the received electric field at x according to (2.1). The total field at x is simply the sum of the contributions of all interrogators at x,

$$E_{Rx} = \sum_{n=1}^{N} A_{i_n} e^{j\phi_n} e^{jkx\sin\theta_n}. \tag{2.3}$$

The retransmitted electric field at x is again the phase-conjugated version of the received field (2.3),

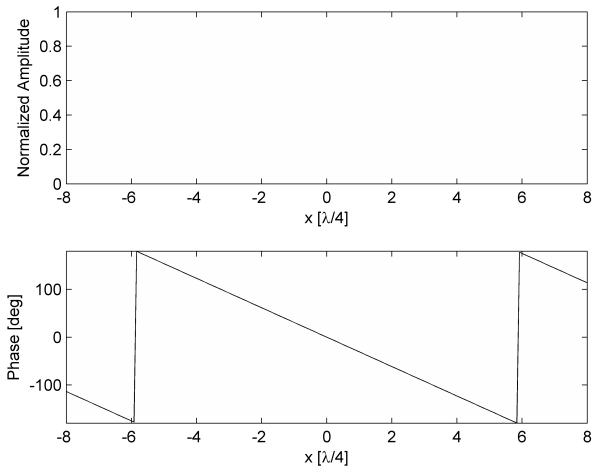

Figure 2.3: Electric field, E_{Tx}, due to a single interrogator at $\theta = 20°$

$$E_{Tx} = \sum_{n=1}^{N} A_{i_n} e^{-j\phi_n} e^{-jkx\sin\theta_n}. \tag{2.4}$$

2.2.1 Single Interrogator Case

For the simplest case, that of a single, plane-wave interrogator, arriving with unity amplitude and phase $\phi = 0$ at the center of the array,(2.1) and (2.2) become,

$$E_{Rx} = e^{jkx\sin\theta} \tag{2.5}$$

and

$$E_{Tx} = e^{-jkx\sin\theta}. \tag{2.6}$$

Fig. 2.3 shows the amplitude and phase of the electric field across the array as determined by (2.6), when the interrogator is placed at $\theta = 20°$. As expected there is a

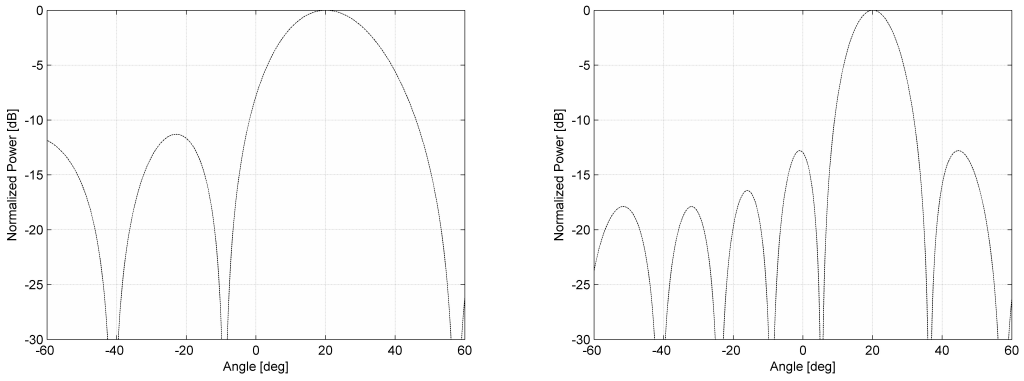

(a) (b)

Figure 2.4: Predicted RCS for a (a) four-element and (b) eight-element PCA in response to a single interrogator at $\theta = 20°$

constant, unity amplitude and a constant phase gradient across the array. Using the electric field at each array element, the PCA's radiation pattern can be determined. Fig. 2.4 shows the predicted bistatic RCS for a single interrogator for a four-element and eight-element array. These will later be compared with experimental results.

2.2.2 Double Interrogator Case

For the case of two equidistant, plane-wave interrogators, arriving in phase with unity amplitude, at angle $\pm\theta$ with respect to the array normal, (2.4) becomes,

$$\begin{aligned} E_{Tx} &= e^{-j\phi}e^{-jkx\sin\theta} + e^{-j\phi}e^{+jkx\sin\theta} \\ &= e^{-j\phi}(e^{-jkx\sin\theta} + e^{+jkx\sin\theta}) \\ &= 2e^{-j\phi}\cos(kx\sin\theta) \end{aligned} \tag{2.7}$$

Taking the phase at the center of the array to be $\phi = 0$ then,

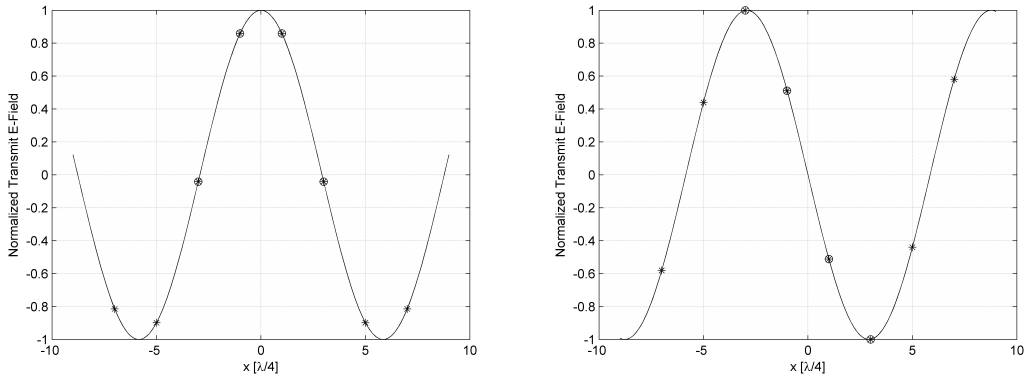

(a) (b)

Figure 2.5: Normalized transmitted electric field for (a) in-phase (b) out-of-phase interrogators at $\pm 20°$. The x-axis is in units of quarter wavelengths. The circles denotes the electric field at each element of a four-element array, and the asterisks represent the eight-element case.

$$E_{Tx} = 2\cos(kx\sin\theta). \tag{2.8}$$

In the case where the two interrogators arrive out of phase at the array center, (2.4) becomes

$$\begin{aligned} E_{Tx} &= e^{-jkx\sin\theta} + e^{-j\pi}e^{+jkx\sin\theta} \\ &= e^{-jkx\sin\theta} - e^{+jkx\sin\theta} \\ &= -2j\sin(kx\sin\theta). \end{aligned} \tag{2.9}$$

The odd (sine) and even (cosine) symmetry of the transmitted electric field across the array, as indicated by (2.8) and (2.9), helps to explain the effects of the phase difference between interrogators as well as the effect of angle of incidence on PCA performance. Fig 2.5(a) depicts the electric field distribution across the array as determined by (2.8), if the array is interrogated by two in-phase interrogators situated at $\theta = \pm 20°$. Since the electric

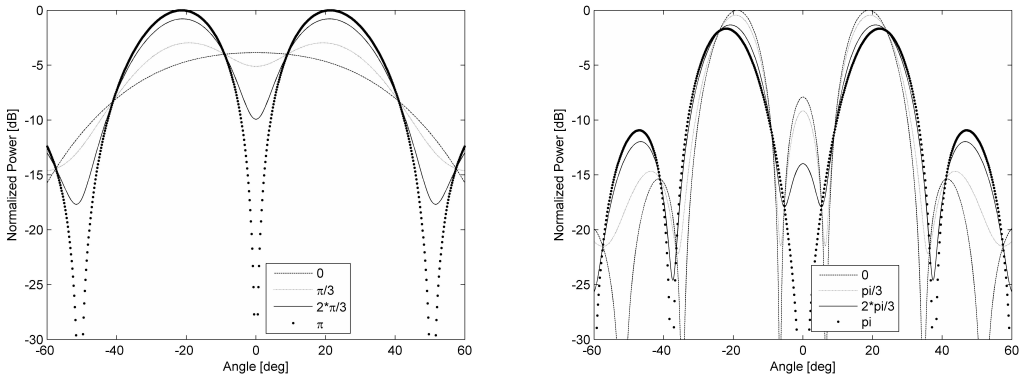

(a) (b)

Figure 2.6: Predicted multistatic RCS as a function of phase difference between interrogators with $\theta = \pm 20^\circ$ on (a) a four-element PCA and (b) an eight-element array.

field is symmetric about the array center, opposite elements will combine in phase, creating a central peak. In contrast, if the array is interrogated by two out-of-phase interrogators at $\theta = \pm 20^\circ$, the electric field distribution across the array is as depicted in Fig. 2.5(b). The anti-symmetric nature of the electric field distribution causes opposite elements to be phase reversed from one another, creating a central null.

Fig. 2.6(a) shows the predicted multistatic RCS, for a four-element PCA, as a function of the phase difference between interrogators. When the interrogators are 180° out of phase, there are two distinct retrodirected beams in the direction of the interrogators, representing desired array operation. However, as the phase difference deviates from the out-of-phase condition, it becomes more difficult to resolve the beams, until finally the two beams morph into a single broad beam for the in-phase condition. This behavior is consistent with the field characterization in Fig. 2.5.

The ability to resolve multiple interrogators has implications towards security. With two distinct beams pointing at each interrogator, there is less chance of eavesdropping.

However, just because the main beam of the array does not point towards the desired target does not necessarily mean that communication between the PCA and the target cannot occur. A receiver does not care about an antenna's radiation pattern so long as there is enough power to close the link. To see how changes in array performance affect the communication system as a whole, the link budget must be examined. Lower gain in the direction of the target must be compensated with an increase in the transmitted power: if an isotropic element radiating 0 dBm of power closes the link, so will an antenna with 10 dBi of gain (in the direction of the target) transmitting with -10 dBm of power. To determine how phase difference between interrogators affects quality of the link, the difference in the power transmitted in the desired direction must be examined. From Fig. 2.6(a) it can be seen that there is a 4.6 dB difference in the power transmitted in the desired direction ($\pm 20^\circ$) between the out-of-phase and in-phase case.

Fig. 2.6(b) shows the same kind of plot, but for an eight-element array. Again, when the interrogators are 180° out of phase, there are two distinct retrodirected beams. However, as the phase difference decreases to zero, a lobe forms at the center of the array pointing in the direction of the array normal. The difference in the transmitted power in the direction of interest between the out-of-phase and in-phase case is 1.9 dB. From these results, it is clear that the phase difference between the interrogators at the center of the array has an impact on the PCA's beam pointing.

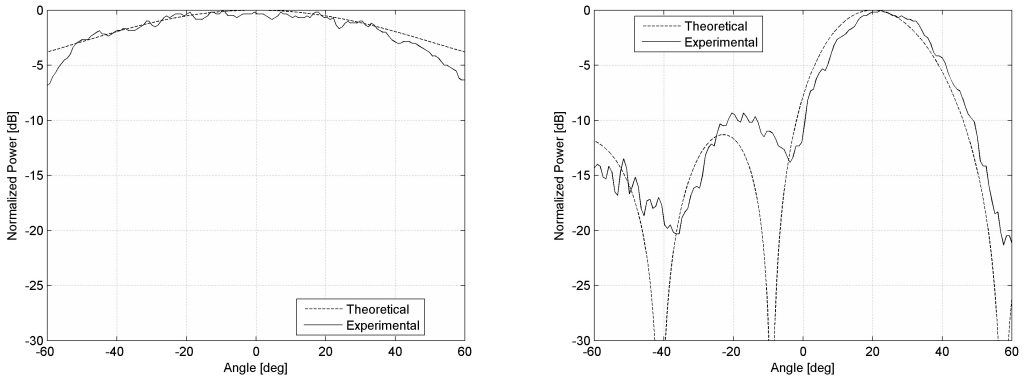

(a) (b)

Figure 2.7: (a) Monostatic RCS and (b) bistatic RCS with interrogator at 20° for the four-element PCA.

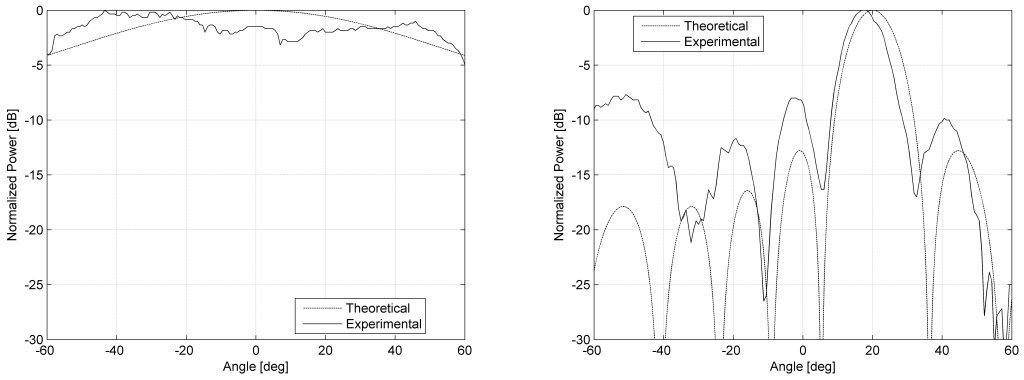

(a) (b)

Figure 2.8: (a) Monostatic RCS and (b) bistatic RCS with interrogator at 20° for the eight-element PCA.

2.3 Experimental Verification

2.3.1 Array Characteristics

A $\lambda/2$ spaced, eight-element PCA using the same architecture as the PCA in [9], was fabricated. The mixer board and power dividers were fabricated on Rogers RO3006 ($\epsilon_r = 6.15$, thickness $= 0.64$ mm) and the antenna array was fabricated on Rogers RT/Duroid 5580 ($\epsilon_r = 2.2$, thickness $= 0.64$ mm). A similar four-element PCA was used to make the four-element PCA measurements. Both PCAs respond to interrogating signals at 6.01 GHz with a retrodirected 5.99 GHz signal. The frequency offset between the interrogating and retrodirected signal allow them to be distinguished on a spectrum analyzer. Monostatic and bistatic RCSs are shown in Figs. 2.7-2.8. The bistatic pattern for the four-element array interrogated at 20° (Fig. 2.7(b)), matches well with the predicted pattern. The main lobe of the eight-element array matches well with theory (Fig. 2.8(b)). The discrepancy in the side lobe levels and null depths is due to a measured amplitude imbalance among the array elements that was confirmed by simulation, as well as the likely multipath caused by carrying out the measurement outside of an anechoic chamber.

Several multistatic RCS experiments were carried out using the general setup in Fig. 2.9. The two interrogating horn antennas, at equal angles (θ) from the array normal, are fed through a 1:2 power divider from a single RF source to ensure that the antennas are fed in phase with equal power. The PCA's response patterns are measured using a receive horn connected to a spectrum analyzer. Three variables are investigated: phase imbalance, incident angle, and amplitude imbalance. Measurements were taken on both the eight- and four-element arrays to verify the analysis.

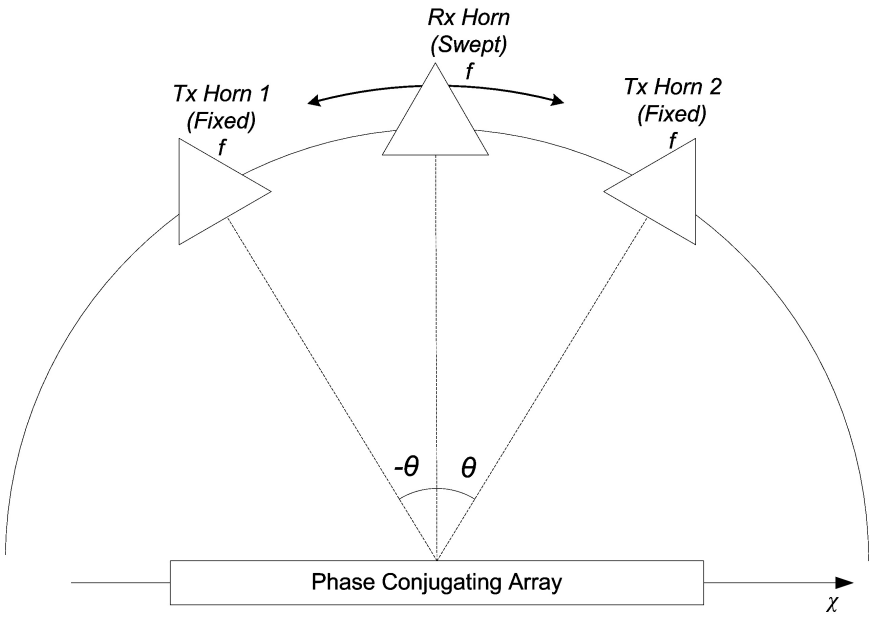

Figure 2.9: General experimental setup.

2.3.2 Effects of Phase Difference Between Interrogators

To verify Fig. 2.6 experimentally, the in-phase and out-of-phase cases were tested. The test set up for the in-phase case has the two interrogators equidistant from the center of the PCA so the two signals arrive in phase. For the out-of-phase case, Tx Horn 2 is placed $\lambda/2$ (2.5 cm) further away from the PCA than Tx Horn 1. The $\lambda/2$ difference in the path length between Tx Horn 1 and Tx Horn 2 is small compared to the total distance between the transmit horns, so the change in signal amplitude from Tx Horn 2 due to the path loss over the extra propagation distance $\lambda/2$ is negligible.

The results in Fig. 2.10 confirm the findings of Fig. 2.6(a), i.e. that the phase difference between the signals has a significant effect on beam resolution. In Fig. 2.10(a), the PCA's response to two interrogators at $+20^\circ$ and -20° arriving out of phase is retrodirected

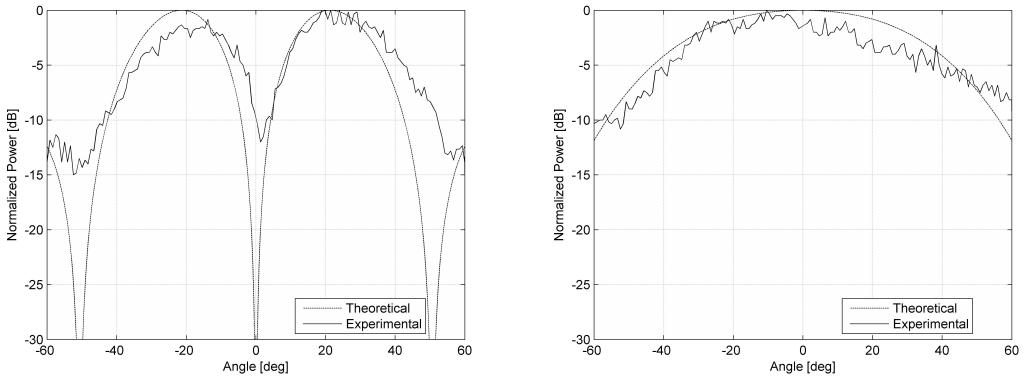

(a) (b)

Figure 2.10: Far-field multistatic RCS for a four-element PCA interrogated by (a) two out-of-phase sources with $\theta = \pm 20°$, (b) two in-phase sources with $\theta = \pm 20°$.

back to each interrogator. In contrast is Fig. 2.10(b), where the signals arrive in phase, the PCA's response consists of a wide, broadside pointing beam with a 2 dB beamwidth of 62.7°, clearly showing the PCA is not retrodirecting.

The performance degradation for the in-phase case is because the four-element array field configuration in Fig. 2.5(a), the outer elements are weighted significantly less than the inner elements. The inner two elements have a normalized electric field intensity of .86, while the outer two elements have a normalized electric field intensity of 0.04. The unequal balance of the elements causes the four-element array to appear as an in-phase, two-element, broadside array, showing that the PCA is not operating as intended.

The eight-element PCA results in Fig. 2.11 match well with the predicted patterns in Fig. 2.6(b). The predicted null appears in the out-of-phase scenario and the predicted central lobe appears in the in-phase scenario. The deviation from the theoretical results is due to amplitude imbalance among the array elements, which through simulation was

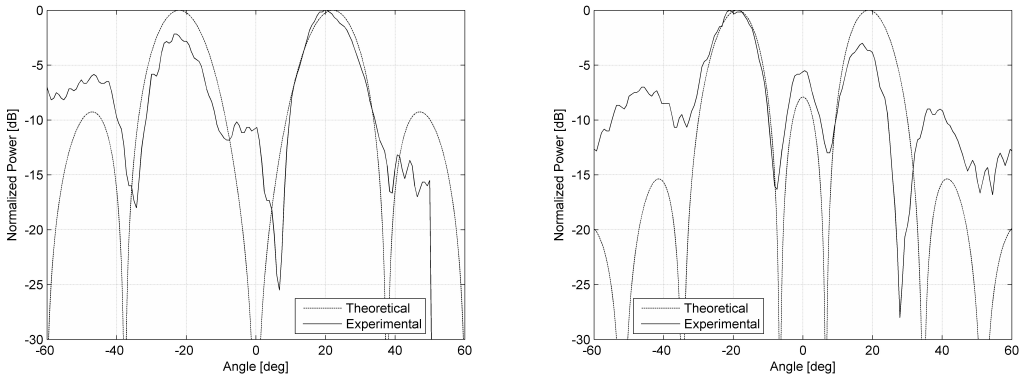

(a) (b)

Figure 2.11: Far-field multistatic RCS for a eight-element PCA interrogated by (a) two out-of-phase sources with $\theta = \pm 20°$, (b) two in-phase sources with $\theta = \pm 20°$.

confirmed to cause higher side lobes and shallower nulls, along with the environment in which the measurements were taken and circuit radiation. These results also confirm the expected increase in performance due to the increased aperture of the array.

Fig. 2.12 shows how the phase difference between the interrogating signals affects the transmitted electric field for the same special case examined in (2.8) and (2.9). As the phase difference between the incident waves increases, the amplitude of the transmitted electric field gets translated horizontally going from $|\cos|$ to $|\sin|$.

2.3.3 Effect of Interrogator Incident Angle

To determine the effect of different incident angles, the angle (θ) for each interrogator with respect to the PCA normal in Figs. 2.10 and 2.11 was changed from 20° to 10°, and the results are shown in Figs. 2.13 and 2.14. Again, as expected, the eight-element array has less beam pointing error than the four-element array. The difference between the theoretical and measured results in the eight-element PCA array are attributed to ampli-

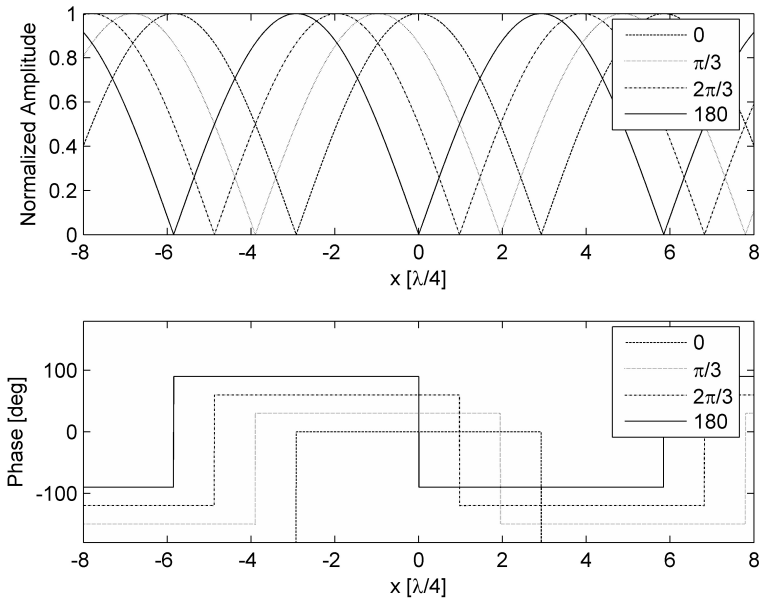

Figure 2.12: Effect of phase difference between interrogators on transmitted electric field.

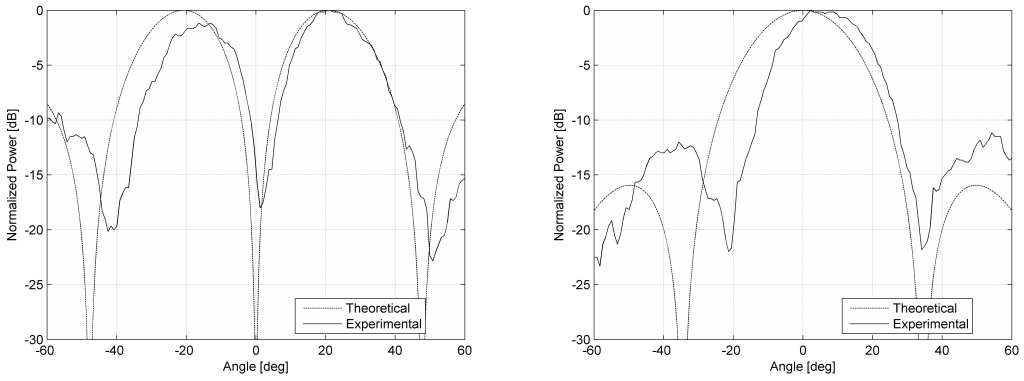

(a) (b)

Figure 2.13: Far-field multistatic RCS for a four-element PCA interrogated by (a) two out-of-phase sources with $\theta = \pm 10°$, (b) two in-phase sources with $\theta = \pm 10°$.

tude imbalance across the array. Comparing Figs. 2.11(b) and 2.14(b), as θ decreases, the beam-pointing error increases significantly when the interrogators arrive in phase.

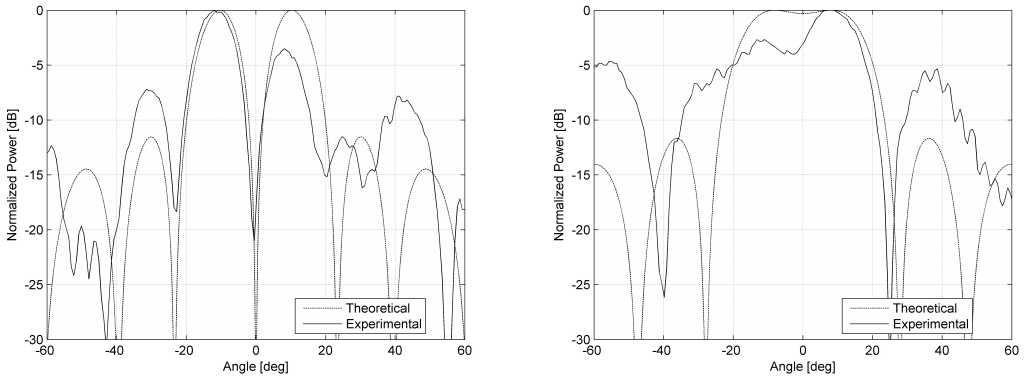

(a) (b)

Figure 2.14: Far-field multistatic RCS for a eight-element PCA interrogated by (a) two out-of-phase sources with $\theta = \pm 10°$, (b) two in-phase sources with $\theta = \pm 10°$.

This trend can be explained by examining the graph of (2.8). The angle between the interrogators affects the period of the cosine. As θ decreases, the period of (2.8) increases, effectively stretching the graph in x as shown in Fig. 2.15. If (2.8) is stretched enough and the number of elements is small enough, all of the elements will radiate in phase and the RDA will not retrodirect. To form multiple beams, the formation of a null is required, so the array must have elements radiating out of phase with one another.

To demonstrate that the PCA can respond to any two interrogators, not just those located at equal angle with respect to the array normal, a pattern was taken with interrogators at $-40°$ and $10°$ arriving in phase at the array center. The results are shown in Fig. 2.16 indicating that the array can indeed steer towards those angles.

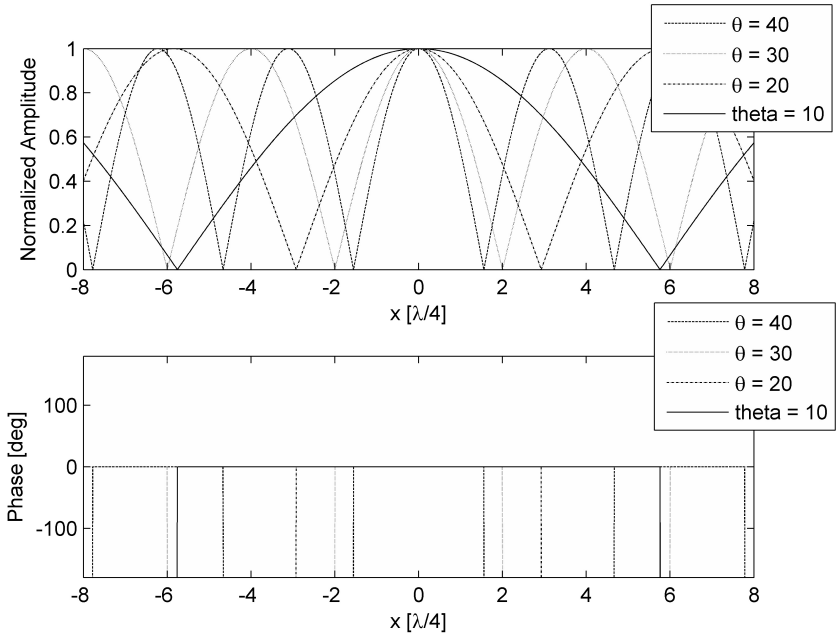

Figure 2.15: Effect of incident angle on transmitted electric field.

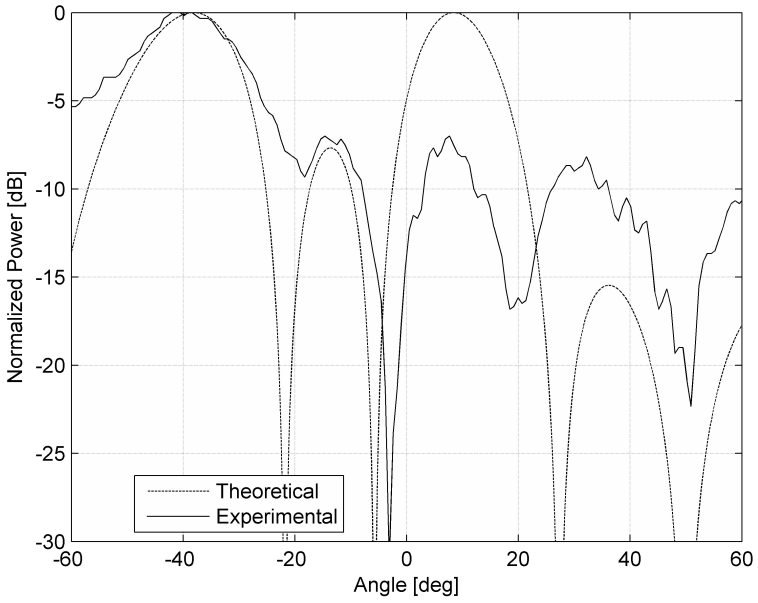

Figure 2.16: Multistatic RCS of an eight-element PCA interrogated by two in-phase sources located at $-40°$ and $10°$.

Chapter 3

An Interleaved Inter-Element Phase-Detecting, Phase-Shifting Retrodirective Array for Interference Rejection

3.1 Introduction

With the ever increasing use of wireless technology, the frequency spectrum is becoming more and more crowded. As the RF environment becomes cluttered with mobile devices, interference between devices becomes more common. Interference-rejection capabilities built into the antenna front end of wireless devices can help to increase the signal-to-noise ratio (SNR) and increase spectral efficiency.

The previous chapter considered scenarios in which an RDA is interrogated by multiple interrogators, and it is desired to respond to each interrogator. This chapter considers just the opposite: the RDA is interrogated by multiple interrogators but it is not desired to respond to each one because they are interferers or eavesdroppers. An interferer is a source that inadvertently interrogates the RDA; communication with the interferer is not desired and any signals emanating from the interferer and received by the RDA will have the undesired effect of decreasing the signal-to-interference ratio (SIR) of the communication system. An eavesdropper is an RF system, either passive or active, whose purpose is to steal information by intercepting communications. A passive eavesdropper does not transmit any RF signals, but just passively collects RF signals incident upon it. An active eavesdropper, much like an interferer, interrogates the RDA, with the intent to elicit a response from the RDA to steal information.

In the situation presented in Fig. 3.1, a mobile phone (containing an RDA) is communicating with a cell tower while at the same time the computer is transmitting at the same frequency as the cell tower. In this case the computer represents an interferer. Fig. 3.2 shows an example of a passive eavesdropper. In this scenario, communications between the vehicle and the aircraft are being intercepted by the eavesdropping device disguised as a rock. The objective of this chapter is to present an RDA capable of steering a beam to an intended target (cell tower/aircraft) while forming a null toward an interferer (computer) or eavesdropper (rock).

A previous RDA architecture that mitigates the potential for passive eavesdropping using a beam-steering RDA and a null-steering RDA is presented in [16]. The beam-steering

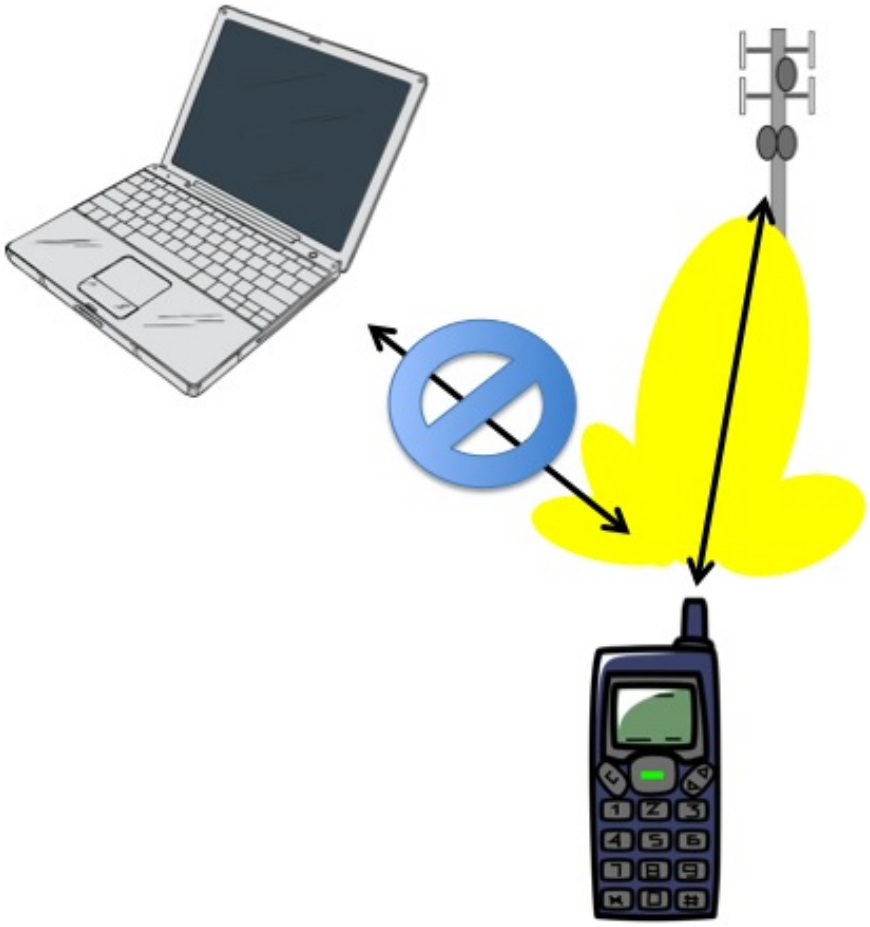

Figure 3.1: A mobile phone user in the presence of an interferer.

RDA communicates with the target, directing its information-encoded signal toward the interrogator. The second null-steering RDA serves as a jammer, sending a high-power jamming signal in all directions, except in the direction of the interrogator, toward which it steers a null. This design was streamlined in [17], requiring only a single front-end array. The net effect of these arrays on eavesdroppers is equivalent to trying to listen in to a conversation between two people while loud music is being blasted in your direction. While these two architectures do help to mitigate the possibility of eavesdropping, they do so by

Figure 3.2: A vehicle communicating with an aircraft in the presence of an eavesdropper.

sending out a jamming signal in all directions, wasting power and adding to an already crowded RF spectrum. These architectures also cannot reduce the effect of interferers since there is no mechanism in place to form a null in a particular direction.

An architecture that can reduce the potential for both eavesdropping and interference was first proposed by D. Goshi et al. in [18]. By using interleaved sub-arrays of mixer-based RDAs the architecture is able to steer both a beam and a null in radiation pattern of the transmitted signal. By steering the null in the direction of an interferer the SNR of the system is improved. However, this architecture's use of heterodyne mixing

results in a R^4 path loss.

This chapter presents an RDA design capable of steering a retrodirected beam toward an interrogator while at the same time forming a null in another direction, with only an R^2 path loss. This is accomplished by combining the interleaved nature of [18] with [6], to decouple the incoming signal from the outgoing signal, reducing the path loss to R^2. The architecture presented in [6] was chosen because it is the first RDA that was demonstrated to respond to multiple interrogators while incurring only an R^2 path loss. The identification friend or foe (IFF) scheme to detect interferer/eavesdroppers and the control circuit for forming a null in their direction is left as future work.

3.2 Design

With a single one-dimensional array, forming a single null in a desired direction is relatively simple. The array factor for an N-element, uniform array is given by

$$AF(\psi) = \frac{\sin\left(\frac{N}{2}\psi\right)}{\sin\left(\frac{1}{2}\psi\right)}, \tag{3.1}$$

where $\psi = kd\sin\theta + \phi$, $k = 2\pi/\lambda$, d is the spacing between elements, and ϕ is the phase difference between elements. Fig. 3.3 shows the geometry involved. A null occurs when (3.1) goes to zero, or equivalently when $\psi = 2\pi/N$. So for a two-element array, with $N = 2$, the proper array phasing is determined by

$$\phi = -kd\sin\theta + \pi. \tag{3.2}$$

Though it is relatively simple to steer a null with a single one-dimensional array, steering

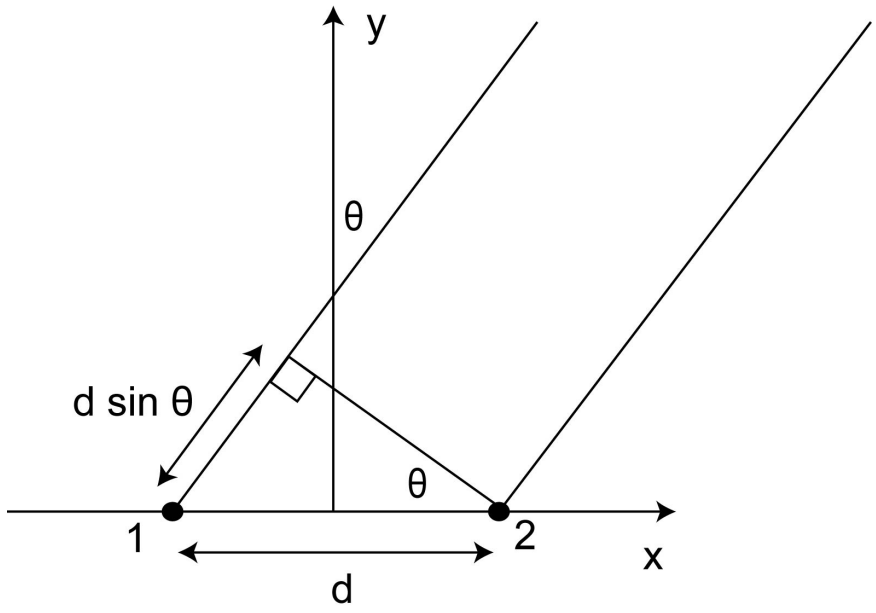

Figure 3.3: Geometry for null-steering calculations

a null in one direction while at the same time steering a beam in another is a much more daunting task that requires the use of beam-forming algorithms such as the one in [19].

To allow the array to retrodirect to one interrogator while steering a null in another direction, two four-element, one-dimensional, retrodirective sub-arrays are interleaved with each other as shown in Fig. 3.4. Each sub-array unit by itself is a fully functioning RDA, but by properly offsetting each sub-array and introducing the correct phase shift, the two sub-arrays interfere destructively to form a null. Because each retrodirective sub-array responds identically (though independently) to the incoming signals, each sub-array can be considered as a single element in a two-element array. Using this two-element model of the array, the null's direction can still be controlled according to (3.2) with the exception that d now represents the offset between the two sub-arrays.

In the scenario depicted in Fig. 3.1, each retrodirective sub-array of the envisioned

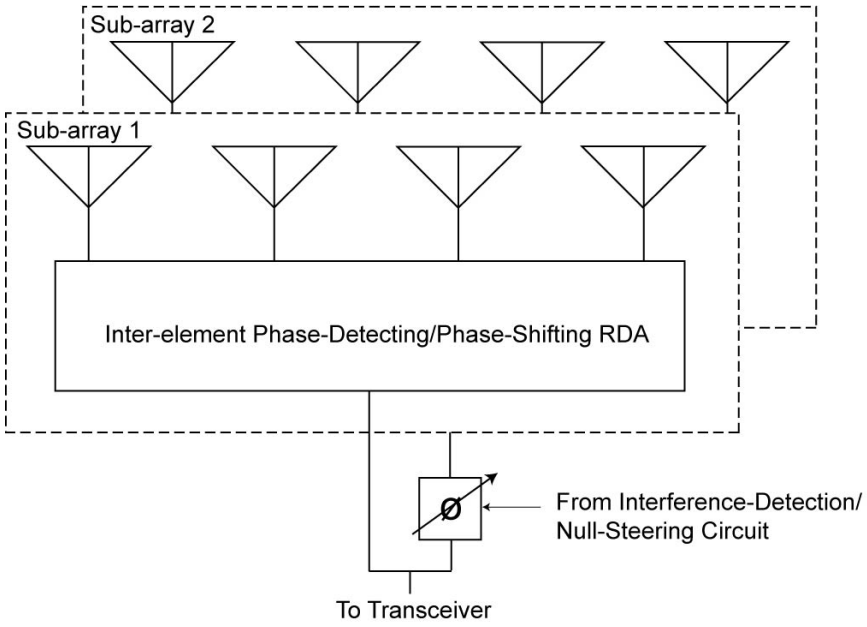

Figure 3.4: Schematic of the interleaved inter-element phase-detecting, phase-shifting retrodirective array for interference rejection.

interleaved RDA located on the mobile phone responds to interrogation by both the cell tower and the computer. However, by virtue of the offset between the two sub-arrays, a null can be steered in the direction of the computer effectively canceling the beam formed in that direction. If each retrodirective sub-array could not respond to multiple interrogators, a null could still be formed in the direction of the interferer, but the main beam would not necessarily be pointing toward the intended target.

To see why the ability to respond to multiple interrogators is required for accurate beam pointing, array theory must be considered. The total electric field of a phased array is simply the array factor, AF, multiplied by the element pattern. If each retrodirective sub-array is imagined to be an element in a two-element array, the element pattern for the interleaved array on the mobile phone in Fig. 3.1 would consist of two beams, one pointing toward the cell tower and one pointing toward the computer. A properly placed

phase shift between the two retrodirective sub-arrays as determined by (3.2) would create an array factor with a null pointing in the direction of the computer. The total electric field by virtue of the product of the element pattern and array factor consists of a beam pointing in the direction of the cell tower and a null in the direction of the computer. The relationship between the element pattern, array factor, and total radiation pattern can be seen in Fig. 3.5. If the two retrodirective sub-arrays are not able to respond to multiple interrogators, the null in the direction of the computer would still remain because that is solely dependent on the array factor (or phasing between the two arrays); however the sub-array pattern would point to some intermediate angle between the cell tower and computer. The main lobe in the total electric field would therefore not be pointing directly at the intended target, in this case, the cell tower. Similar to the results of the last chapter, just because the main lobe of the interleaved array does not point directly at the intended target does not mean that the target cannot communicate with the RDA. However, this does represent an inefficient use of RF power, reducing the power received by both the RDA and target as well as the signal-to-noise ration (SNR).

Conceivably, an identification-friend-or-foe (IFF) scheme could be used with the power-detecting phase-shifting RDA to prevent communication with undesired interrogators. A typical IFF scheme uses identification codes to authenticate an interrogator as a friendly; communications are only opened up with authenticated friendlies. As the array scans its beam it can check for the authentication code. The angle with the highest receive power also receiving an authentic code corresponds to the angle of the intended target. The RDA, in the presence of a single, non-friendly interrogator would reject communications. If

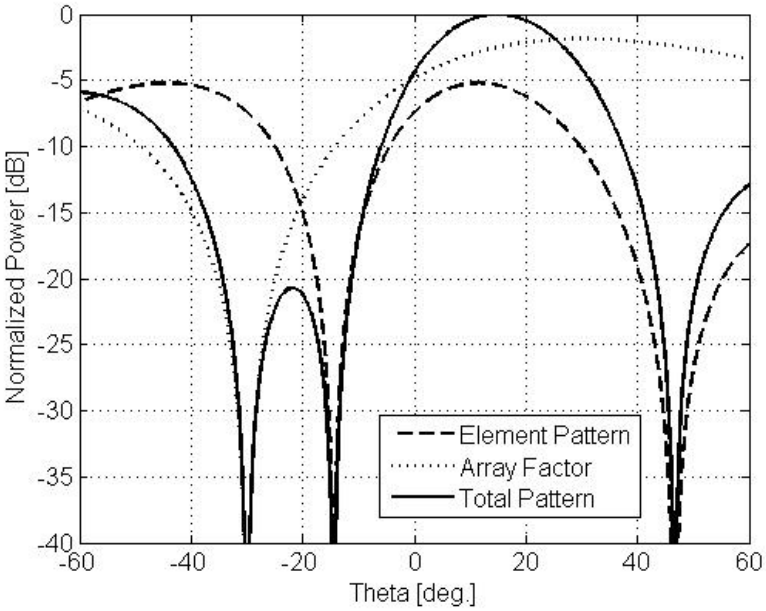

Figure 3.5: Simulated RDA "element" pattern, array factor, and total radiation pattern for an interleaved RDA with interrogators located at $-30°$ and $0°$, and null steered to $-30°$.

there were a friendly interrogator as well as interferers or eavesdroppers, the RDA would point its beam toward the friendly, but could not steer a null toward the interferer or eavesdroppers. Since there is no null in the direction of the interferer there is no reduction in the level of intereference, or if it were an eavesdropper there is no reduction in the signal strength transmitted in the direction of the eavesdropper (for example, the signal in a side lobe).

3.2.1 Retrodirective Sub-Array

Two identical RDAs based on the inter-element phase-detecting/phase-shifting architecture [6] are used as the retrodirective sub-arrays. The inter-element phase-detecting/phase-shifting RDA consists of three main parts: the phase-shifting array, the phase-detecting

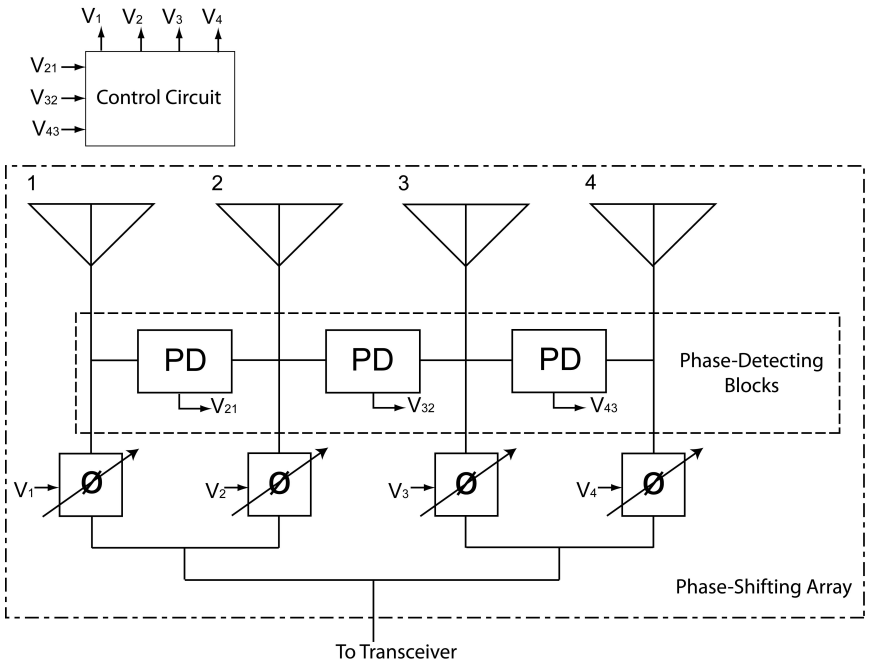

Figure 3.6: Block diagram of the four-element retrodirective array using interelement phase detection and phase shifting from [6].

circuit, and the control circuit. A schematic of the inter-element phase-detecting/phase-shifting array is shown in Fig. 3.6. The phase-shifting network consists of the antenna array, the phase shifters, and the power dividers and associated microwave circuits, and is responsible for distributing and phasing the RF signal. The phase-detecting block measures the phase difference between the incoming signal of two adjacent elements and outputs a voltage proportional to that phase difference. The control circuit takes the outputs of all the phase-detecting blocks and outputs a control voltage to each phase shifter to properly phase the array.

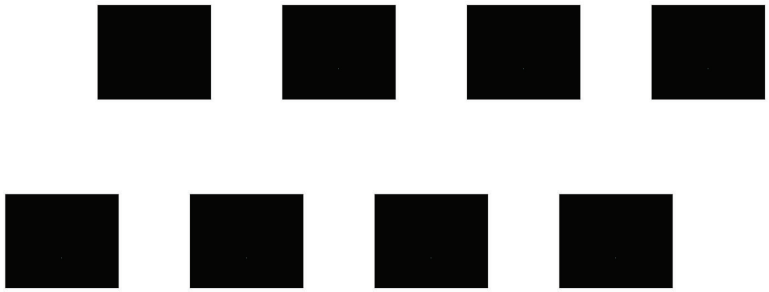

Figure 3.7: Schematic of the patch antenna array.

Phase-Shifting Network

The antenna array used for this system consists of eight, probe-fed, microstrip patch antenna elements designed in ADS. The patch antenna is designed to operate with a center frequency of 2.4 GHz with the feed placed to create an input impedance of 50 Ω. Each four-element array has an element spacing of $\lambda/2$. The two arrays are separated by 3.21 cm and offset by 0.77 cm; these distances were chosen, through simulation, to minimize the effect of coupling. A schematic of the final array design is shown in Fig. 3.7. The array was fabricated on Rogers RO4350B substrate ($\epsilon_r = 3.48$, $t = .762$ mm), and is shown in Fig. 3.8.

Fig. 3.9 shows the microwave circuitry for each four-element retrodirective sub-array. As a signal impinges on the sub-array it is received by the patch antenna elements where it passes through a 1:2 Wilkinson power divider. Each of the two resulting ports from the power divider feeds a 90° hybrid coupler. The coupled port of the hybrid coupler syphons off 3 dB of the remaining signal to feed the phase-detector circuit. The hybrid coupler also

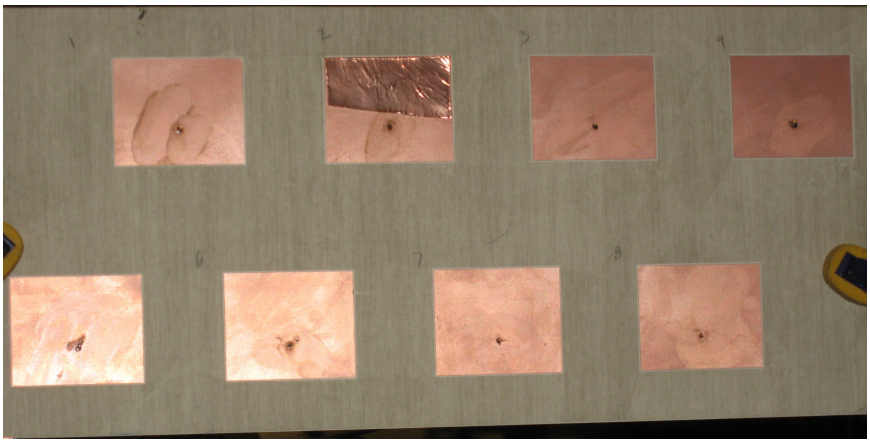

Figure 3.8: Photograph of the final fabricated array.

provides 32 dB of isolation between the transmit signal, going from the transceiver to the antenna elements, and the phase-detecting circuit's input, coming from the antenna elements. The through ports of the two hybrid couplers for each element are recombined using a 2:1 Wilkinson power combiner, and pass through a Pulsar ST-21044 phase shifter. After the signals from each element are properly phase shifted, they are combined using a 4:1 Wilkinson power combiner; this constitutes the output of a single retrodirective sub-array. The elements shown in Fig. 3.9, with the exception of the the 4:1 Wilikinson power divider at the bottom, were all fabricated on the same board using Rogers RT 6010LM ($\epsilon_r = 10.2$, $t = 0.635$ mm) as the substrate.

The only active components in the phase shifting network are the phase shifters. The control circuit outputs a control voltage to each phase shifter. Fig. 3.10 shows the characteristic curve of the phase shifter, showing how the phase shift varies with the applied voltage. In contrast to [6], only one Pulsar ST-21044 is used for each element. When using only a single phase shifter, the linear range of the phase shift versus voltage curve does not

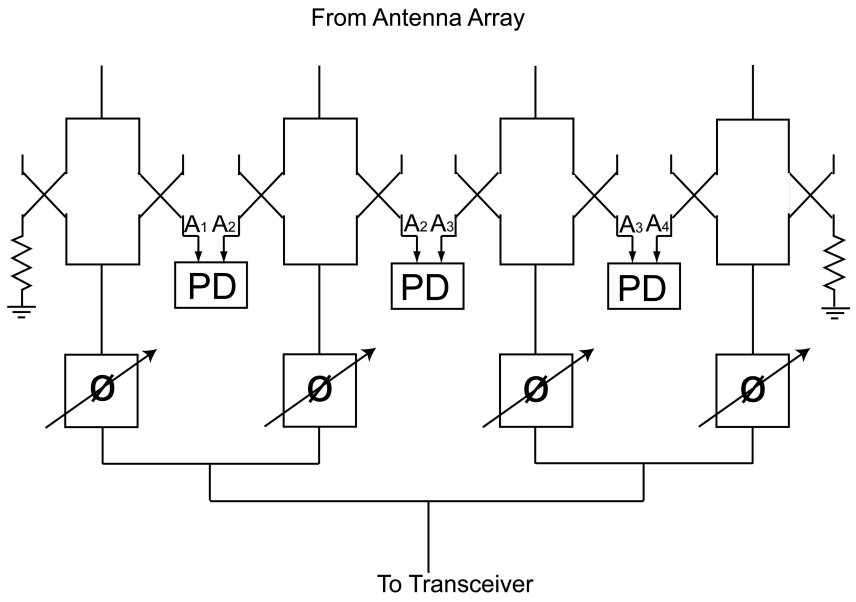

Figure 3.9: Schematic of the phase-shifting array and phase detecting blocks from [6].

cover the maximum amount of phase shift that is needed for the four-element sub-array (540°). It is desired to remain in the linear region of the phase shift versus voltage curve to make implementation of the control circuit simpler.

To compensate for the lack of linear range in a single phase shifter, a wrapping circuit must be used to "wrap" the phase. Because of the cyclical nature of the phase, a 375° phase shift can be represented instead by a 15° phase shift, for example. Since only a 360° range is needed for phase shifting, the range from $0V - 6.63V$ $(-136° - 224°)$ is used. Any voltage over 6.63V is wrapped. The wrapping circuit is implemented using a simple comparator circuit, shown in Fig. 3.11, that carries out

$$V_{PS\,CTL_i} = \begin{cases} V_i & \text{for } V_i \leq V_{360°} \\ V_i - V_{360°} & \text{for } V_{360°} < V_i \end{cases}, \tag{3.3}$$

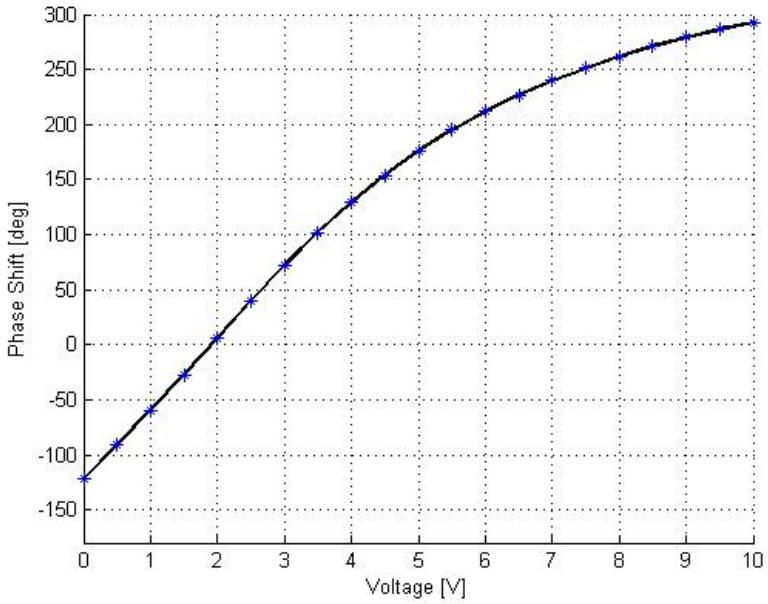

Figure 3.10: Phase shifter characteristic curve.

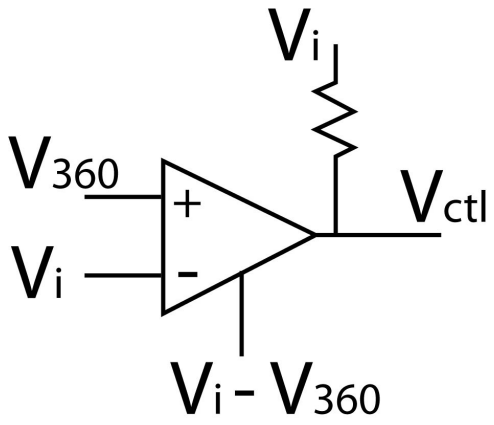

Figure 3.11: Comparator circuit to implement phase wrapping

where V_{PSCTL_i} is the output of the wrapping circuit, V_{360° is the largest voltage on the linear 360° range, and V_i is the input into the wrapping circuit from the control circuit.

Phase-Detecting Circuit

To achieve retrodirectivity, the phase difference between each adjacent pair of antenna elements must be reversed. The first step towards achieving that end is to measure the incoming phase difference between each pair of adjacent elements,

$$\Delta\phi_{(i+1)(i)} \equiv \phi_{(i+1)} - \phi_i, \tag{3.4}$$

where ϕ_i is the phase on the i^{th} element with $i = 1$ corresponding to the leftmost element.

This is the role of the phase-detecting blocks. The phase-detecting blocks measure the phase difference between adjacent element pairs and outputs a voltage, $V_{(i+1,i)}$,proportional to that phase difference. That voltage is later used by the control circuit to determine the proper phase-shifter control voltages. There are three phase-detecting blocks in each four-element retrodirective sub-array.

The phase detector used for this block is Analog Devices' AD8302 phase detector. Two phase detectors are needed in each block because the output of the AD8302 phase detector is symmetric with respect to phase. With a single AD8302 chip it is impossible to tell whether the phase difference is positive or negative. The plot of "Theorectical V_A" in Fig. 3.12 shows the ideal characteristic curve of a single AD8302 chip.

To allow a positive phase difference to be distinguished from a negative phase difference, a second phase detector is added, however the second phase detector has a 90° phase shift added to one of the inputs, creating a characteristic curve labeled "Theoretical V_B" in Fig. 3.12. So, if the output of the second phase detector, V_B, is greater than $0.9\,V$, the phase difference is negative; if V_B is less than $0.9\,V$, the phase difference is positive. Comparators are used to create the output voltage of the phase-detecting block, using the

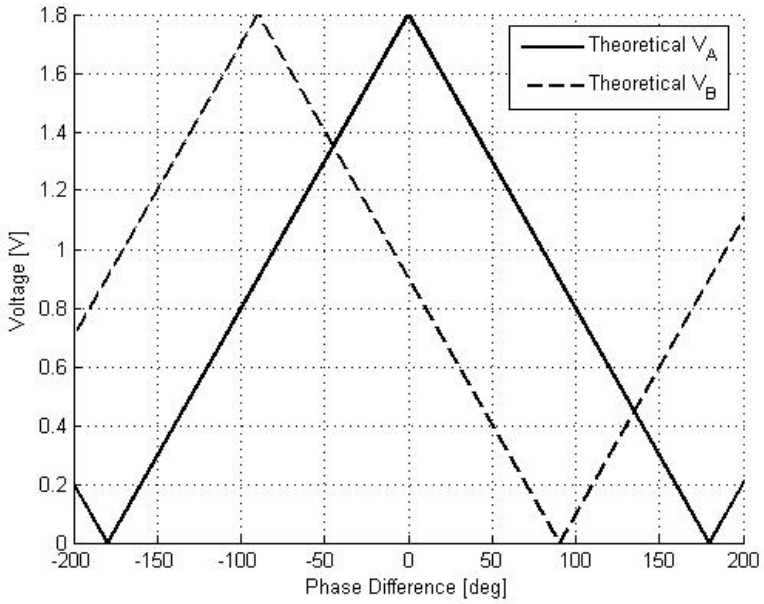

Figure 3.12: Theoretical voltage versus phase difference curves for the two phase detectors in a phase-detecting block.

output of phase detector B to determine if the phase shift should be positive or negative. The comparator creates an output voltage as shown in Fig. 3.5 by implementing:

$$V_{PD} = \begin{cases} V_A - 1.8 & \text{for } V_B \geq 0.9V \\ 1.8 - V_A & \text{for } V_{360^\circ} < 0.9V \end{cases} . \tag{3.5}$$

The schematic of the phase-detecting block between elements 1 and 2 is shown in Fig. 3.13.

Control Circuit

The control circuit is responsible for producing the proper phase-shifter control voltages to properly steer the sub-array. To achieve retrodirectivity, the phase difference between each adjacent pair of antenna elements must be reversed. Because this array operates only on phase differences between elements, a reference phase must be set, so the

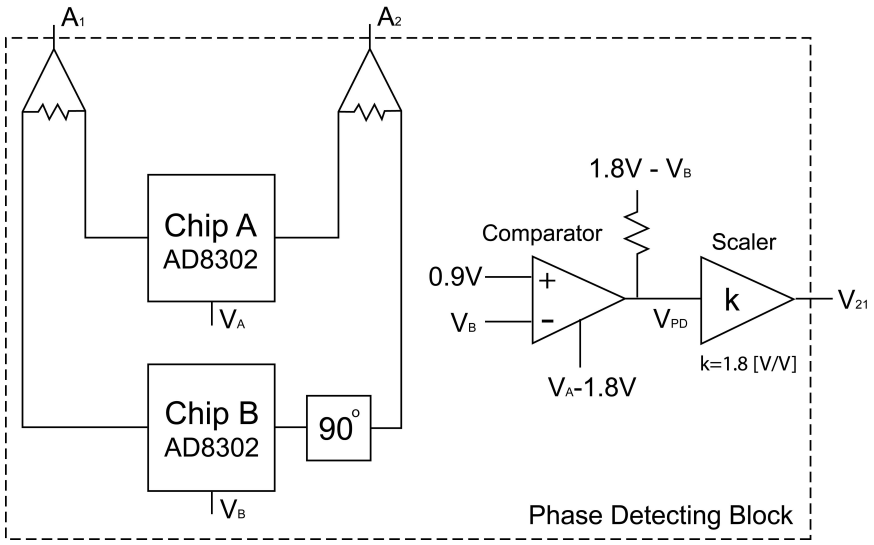

Figure 3.13: Detailed schematic of the phase detecting block between elements 1 and 2, showing the implementation of the two phase detectors and comparator to achieve a 360° detection range.

actual element phases can be determined. The reference phase ϕ_{ref} is chosen to be half of the phase shifter range, or 180°, at the center of the array.

Using the reference phase, ϕ_{ref}, the phase needed at each element to create the retrodirected wave is:

$$\begin{aligned}
\phi_1 &= \phi_{ref} + \frac{1}{2}\Delta\phi_{3,2} + \Delta\phi_{2,1} \\
\phi_2 &= \phi_{ref} + \frac{1}{2}\Delta\phi_{3,2} \\
\phi_3 &= \phi_{ref} - \frac{1}{2}\Delta\phi_{3,2} \\
\phi_4 &= \phi_{ref} - \frac{1}{2}\Delta\phi_{3,2} - \Delta\phi_{4,3}.
\end{aligned}$$

In terms of voltages this becomes:

$$\begin{aligned} V_1 &= V_{ref} + \frac{1}{2}\Delta V_{3,2} + \Delta V_{2,1} \\ V_2 &= V_{ref} + \frac{1}{2}\Delta V_{3,2} \\ V_3 &= V_{ref} - \frac{1}{2}\Delta V_{3,2} \\ V_4 &= V_{ref} - \frac{1}{2}\Delta V_{3,2} - \Delta V_{4,3}, \end{aligned}$$

where V_{ref} is 3.3 V, the voltage that corresponds to the reference phase.

First, a breadboard prototype of the control circuit was created and tested to ensure proper operation. Then, the final control circuit layout, along with the layouts for the comparator circuits of the phase-shifting array and the phase-detecting blocks, were created using EagleCAD and fabricated by Advanced Circuits.

3.2.2 Null Steering

To steer a null a phase shift, in accordance with (3.2) must be introduced between the two retrodirective sub-arrays. Because there was no phase shifter available the phase shift was created using a 1:2 Wilkinson power divider with one output line delayed. The delay line was created to steer a null to $-30°$. Using (3.2) it was calculated that a 124° delay was needed to steer the null. ADS was used to simulate and layout the power divider and phase delay. Fig. 3.14 shows a schematic of the delay line used.

In a real system the delay line would be replaced by a phase shifter to allow for electronic control over the null's location. A separate circuit, not yet designed, would determine direction of the interferer, and, in a manner similar to the control circuit of the sub-arrays, produce the proper voltage to phase the interleaved array to point its null in

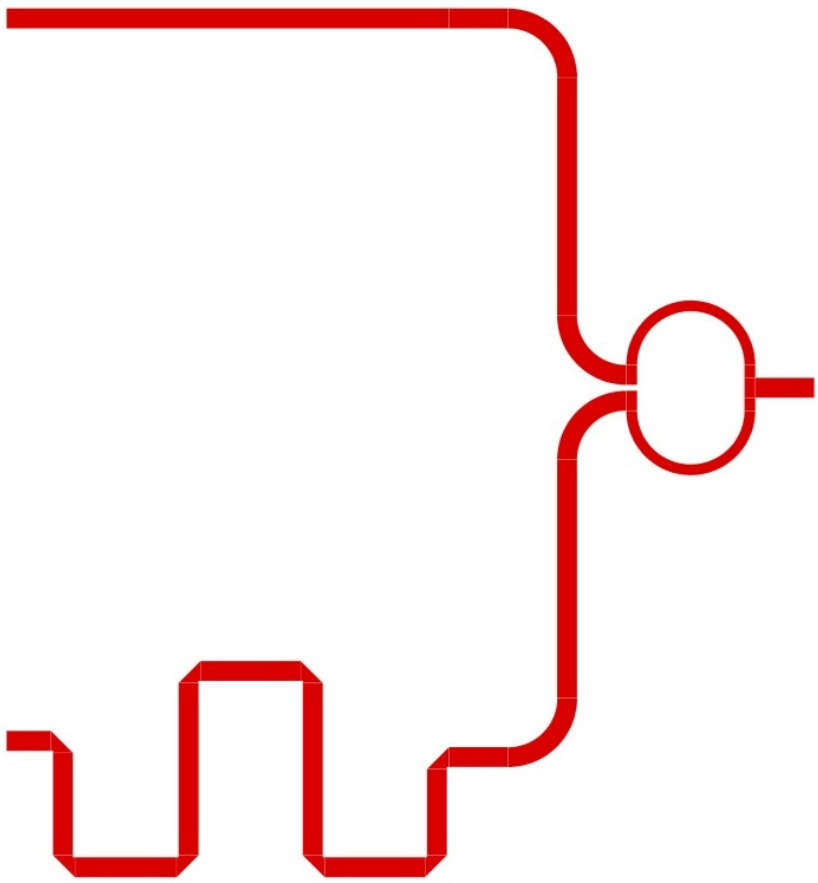

Figure 3.14: Layout of the power divider with phase delay.

that direction.

3.3 Experimental Results

Fig. 3.15 shows the complete array setup. The transmit frequency of the RDA is set to 2.45 GHz with -6.0 dBm of power, with the interrogators transmitting at 2.4 GHz with 13 dBm of power. The first test yielded poor results because the received power from the array fell into the noise floor of the spectrum analyzer. To remedy that problem a low

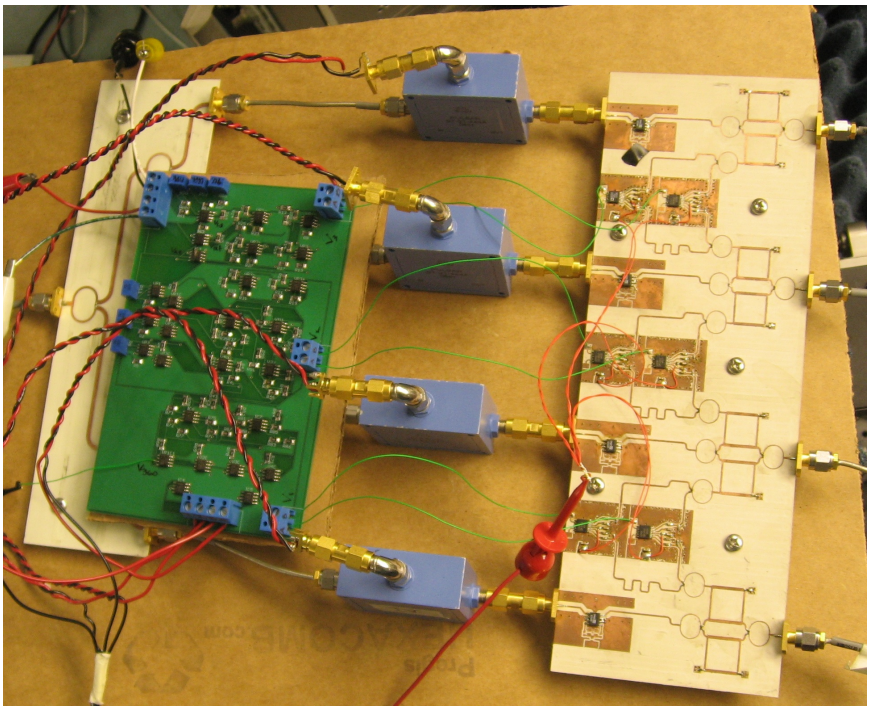

Figure 3.15: Picture of a complete retrodirective sub-array (without antenna array) .

noise amplifier (LNA) was used to amplify the receive horn signal before being input to the spectrum analyzer.

Each retrodirective sub-array was first tested individually to ensure proper operation. Fig. 3.16 shows the bistatic RCS taken for the individual RDAs. After proper operation of the sub-arrays was verified, the full interleaved array was tested with the Wilkinson power divider with 124° phase delay replaced with a standard Wilkinson power divider. When testing the full array the measured bistatic patterns did not match theoretical patterns. Because it was verified that retrodirective sub-arrays were working properly, the disparity must have been due to a phasing error between the two sub-arrays. It was later discovered that the 4:1 Wilkinson power divider that feeds each sub-array did not

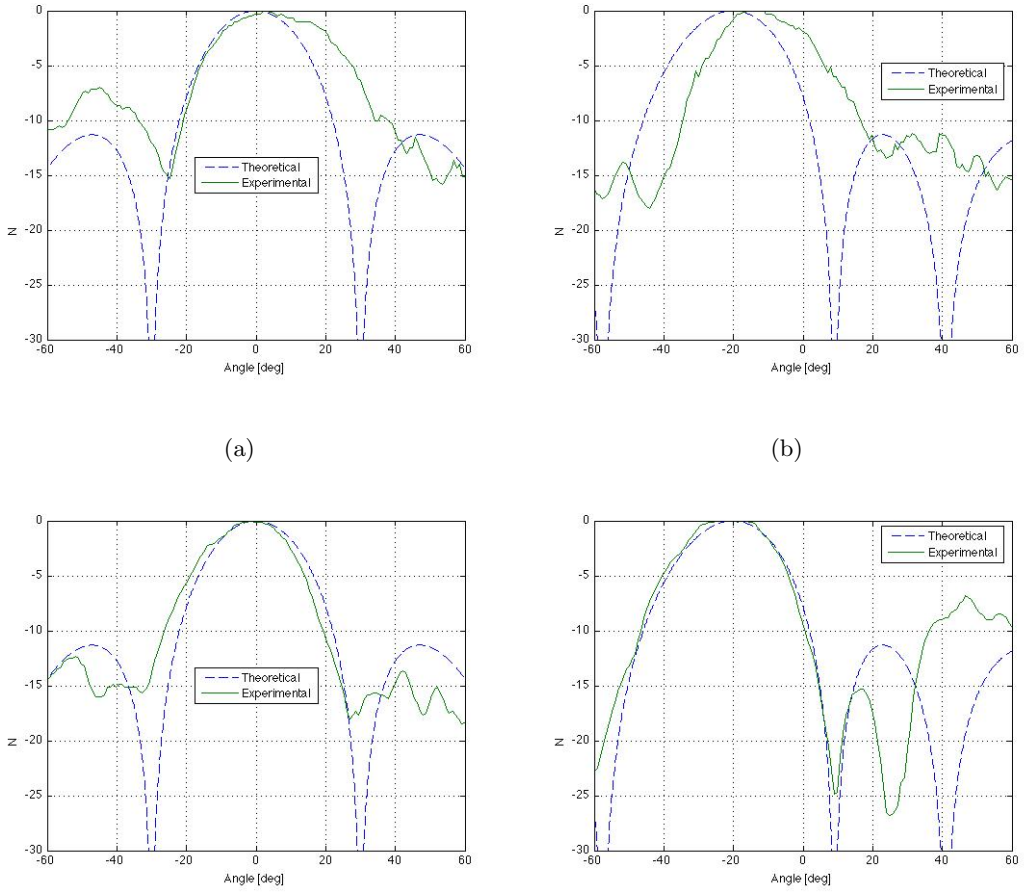

Figure 3.16: Bistatic RCS for sub-array 1 with Bistatic RCS for sub-array 2 with interrogators at (a) 0° and (b) −20°.

have the same phase delay at the output. Two identical power dividers were fabricated and measurements were taken and proper array operation was verified. Fig. 3.17(a) shows a multistatic RCS of the full interleaved array with interrogators located at ±30°.

To demonstrate that the interleaved array could indeed steer a null, the Wilkinson power divider with 124° delay line was connected and a multistaic RCS was taken. Fig. 3.17(b) shows the resulting pattern. The array points its main beam in the direction

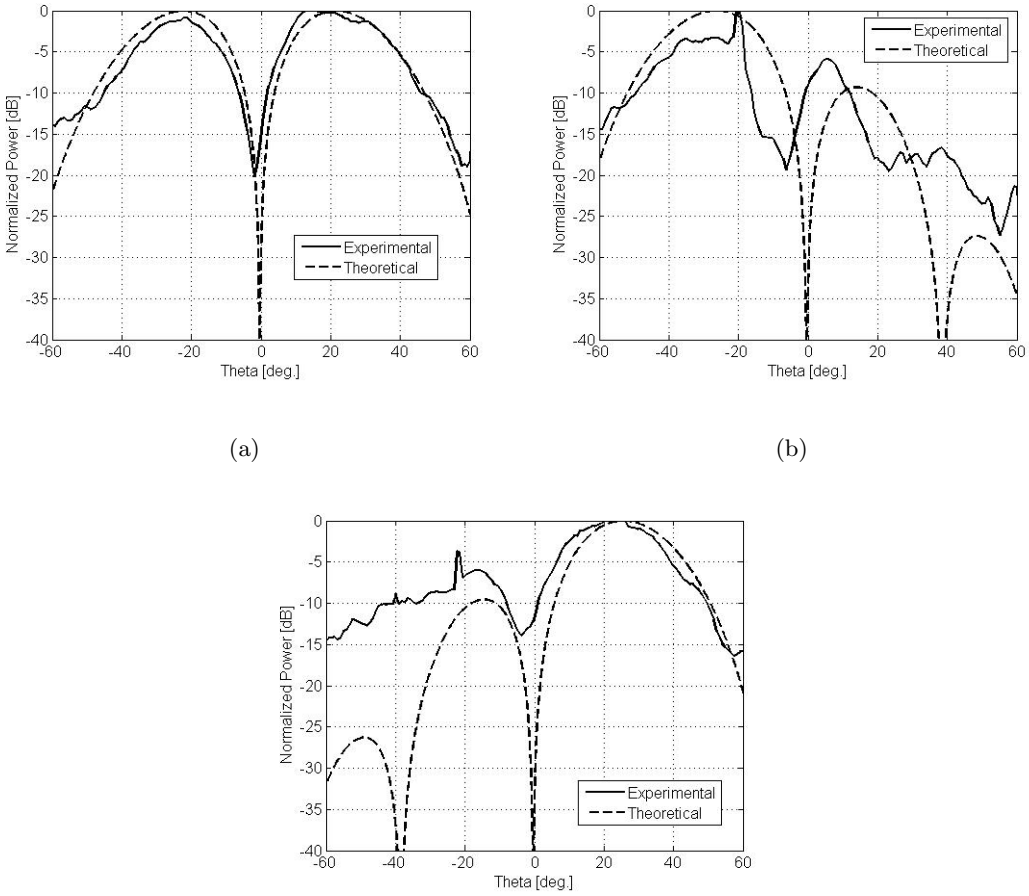

Figure 3.17: Multistatic RCS of the interleaved array with interrogators at ±30° (a) with no null formed, (b) with null steered to 30°, and (c) with null steered to −30°.

of the interrogator located at −30°, albeit with a beampointing error of 10°. The difference in power transmitted to the intended target at −30° and the interferer at 30° is 14.34 dB. Next the Wilkinson power divider with 124° delay line was flipped over, reversing the phase difference between the two arrays, having the effect of steering the null to −30°. The bistatic RCS is shown in Fig. 3.17(c). In this case there is a 7.84 dB difference in the power directed to the intended target versus the interferer.

3.4 Conclusions

This interleaved RDA architecture has demonstrated the ability to steer a null while still being able to retrodirect a beam in the direction of an intended target. However, it must be noted that for this particular architecture the null must be steered manually, meaning the user must operate the null steering mechanism; the null will not automatically direct itself towards an interferer. Future work on this project could include adding circuitry to detect interferers and autonomously steer the null in that direction.

Since two retrodirective sub-arrays are needed to be able to form a null while at the same time steering the beam, this extra functionality comes at the cost of twice the hardware. This means the size, weight, and power (SWAP) requirements of the RDA are doubled. However, if the communication system is transmitting sensitive information and is operating in a interference laden environment, this architecture would provided a substantial improvement on link security and a reduced the burden on the receiving circuitry compared to a standard RDA.

Chapter 4

Conclusions and Future Work

4.1 Conclusions

Retrodirective arrays present an attractive alternative to other types of directive arrays. Their documented self-steering capabilities and multipath mitigation capabilities make them ideal for use in mobile communications. It has been shown in Chapter 2 that phase-conjugating arrays can respond to multiple interrogators. The performance of the PCA will depend on the characteristics of the interrogators (i.e. phase difference between interrogators, angle of incidence, etc.). The variations in performance can be reduced by increasing the array size, so there is a trade off between performance and the array's size, weight, and power (SWaP) requirements.

Though PCAs incur an R^4 path loss making them impractical for mid-range and long-range systems, they can still be used for short-range applications, such as indoor routers. Compared to the monopole antennas that are typically used, the self-steering PCA provides a relatively simple, high directivity alternative. The RDA's directive beam

provides a higher gain than the monopole antennas, offering a stronger link. The ability of PCAs to respond to multiple interrogators means that the link quality can be improved even with multiple users present and also has the benefit of reducing the multipath fading.

Chapter 3 presented an RDA architecture capable of retrodirecting to a single interrogator while forming a null in a different direction, increasing the security of the RDA's link. The architecture presented represents an improvement over previous ones, reducing the path loss incurred and eliminating the loss due to phase conjugating through mixing. Though this architecture, as it stands, cannot identify and steer a null towards an interferer or eavesdropper, it represents a first step toward that end. This architecture comes at the cost of increased size, power consumption, and complexity. However, if security is paramount, this RDA architecture presents an attractive solution.

Although it is difficult to compete with adaptive beam-forming smart antennas in terms of performance, the interleaved inter-element phase-detecting/phase-shifting RDA provides a relatively inexpensive and attractive alternative to smart antennas for power-constrained environments like a CubeSat. Like a smart antenna, the RDA has the ability to autonomously steer a beam while at the same time forming a null, but with a reduced power requirement. Smart antennas require specialized receivers, intensive digital signal processing (DSP) as well as down conversion, analog-to-digital (A/D) conversion, digital-to-analog (D/A) conversion, and up conversion stages at each element [20] making them less feasible for resource-constrained applications. For a four-element array, the power consumption of the smart antennas A/D and D/C converters alone (4.4W) [1] is similar to

[1]Power consumption figure assumes the use of AD ADC71 analog-to-digital converters and AD 7224 digital-to-analog converters.

the total power consumption of the entire interleaved inter-element phase-detecting/phase-shifting RDA (4.33W). The down conversion stage, up conversion stage, and processor would add to the smart antenna's power consumption making the interleaved inter-element phase-detecting/phase-shifting RDA a better choice for power-constrained platforms.

4.2 A Beam-Scanning Liquid-Metal Reflectarray

As stated in Chapter 2, to reduce the amount of beam-pointing error for an RDA, the array size should be increased. But one drawback of current RDA architectures is that for large arrays, the corporate feed networks used to distribute the LO signals become more complicated. With the increased feed network complexity comes increases in both the physical size and ohmic losses. One way to eliminate corporate feed networks from large arrays is to use a spatial feed on a typical RDA [21]. However, because the LO must arrive with the same phase across the entire array, the feed antenna must be in the far field, leading to large propagation losses.

An alternative is to use reflectarrays. A reflectarray is a directive antenna that combines elements of both parabolic reflector antennas and phased arrays [22]. The reflectarray consists of two parts: a reflecting surface and an antenna feed. The reflecting surface is made up of an array of antenna elements, each with a predetermined phase delay. Similar to a parabolic reflector antenna, the reflectarray is fed spatially, so there is no need for bulky power-divider networks, eliminating the ohmic losses associated with the corporate feed networks. The beam of the reflectarray is formed by virtue of a phase shift designed into each antenna element. The phase shift at each element is chosen to create a coherent

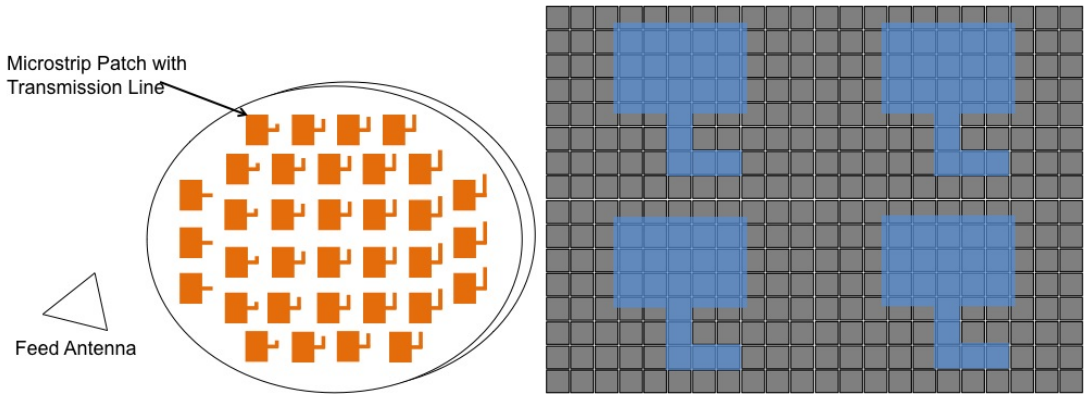

(a) (b)

Figure 4.1: (a) A typical reflectarray using microstrip patch antenna elements with open-circuit stubs (b) Liquid metal reflectarray using EGaIn on a electrode grid.

phase front in the desired direction. However, typical methods used to create the phase shift do not allow dynamic control over the phase, so the radiation pattern of the reflectarray is static. Developing a reflectarray that can steer a beam would be the first step toward creating a retrodirective reflectarray.

One simple implementation of planar reflectarrays uses microstrip components. The antenna is typically a planar antenna, such as a microstrip patch antenna, attached to an open-circuited microstrip transmission line (Fig. 4.1(a)). The signal from the feed antenna impinges on the patch antenna element and travels down the transmission line, where it is reflected upon reaching the end of the transmission line. The reflected signal travels back to the patch antenna and is re-radiated. The phase added to the signal is proportional to the electrical length of the transmission line. However, the phase on each element cannot be dynamically tuned with these fixed-length open-circuited transmission lines.

Recent work has focused on developing beamscanning reflectarrays for more tun-

ability. One approach uses varactor diodes as a loading mechanism for the patch antenna element. By varying the bias on the varactor, the phase of each element can be changed [23]. However, this design requires multiple diodes and biasing circuits for each element, which introduces significant losses and complicates the design of large reflectarrays.

Another approach embeds liquid crystals into the substrate of a reflectarray element. The applied DC bias changes the permittivity, which creates an associated change in phase [24]. However, this results in up to 8 dB of loss in the reflected signal. The phase shift is also limited by the small range over which the permittivity can vary. [25] reported a maximum phase shift of 290°. Colloidal mixtures can also be used to change the dielectric properties of coaxial stubs attached reflectarray elements [26]. This method reports relatively low loss of 1.2 dB with a maximum phase shift of 200°.

The future work proposed here presents a radically different approach to tunable reflectarrays, one that literally changes the shape of the metal pattern itself. Using an electrode grid, liquid metal can be dynamically patterned into various shapes and sizes, much like drawing on an Etch-a-Sketch toy. The phenomena known as electrowetting [27] uses an applied voltage to control a liquid. This technology could be used to implement a tunable reflectarray by forming all of the reflectarray elements out of reconfigurable liquid metal. This not only allows the steering of the reflected beam, but also the tuning of the reflectarray frequency and polarization. The proposed array would consist of a 2D electrode grid covered with patch elements (or other shapes) of different sizes (Fig. 4.1(b)).

If an array of such elements was fabricated, tuning the length of each transmission line would control the phase of each element, causing a beam to be steered. As the phase

shift is created simply by propagation along a transmission line, it will likely have less loss than a varactor diode or liquid crystal based reflectarray. Thus, the proposed approach features dynamic beam steering along with low loss, over a potentially larger range than that of liquid crystal reflectarrays. Manipulation of the geometric shape of the antenna element itself will allow tuning of polarization, frequency, and beamwidth as well.

4.3 Interference Identification and Null-Forming Circuitry

As an extension of the previous chapter's architecture, circuitry to identify interference and control the phase shifter to form a null in the direction of the interferer would make the interleaved architecture fully autonomous. An IFF scheme to distinguish interferers from intended interrogators, and along with the phase and amplitude information, could be used to determine the direction of the interferers. An analog control circuit would then create the proper voltage necessary for the phase shifter to form a null in the direction of the interferer.

Bibliography

[1] W. A. Shiroma, R. Y. Miyamoto, G. S. Shiroma, A. T. Ohta, M. A. Tamamoto, and B. T. Murakami, "Retrodirective systems," in *Wiley Encyclopedia of RF and Microwave Engineering*, K. Chang, Ed. New York: Wiley, Feb. 2005, pp. 1681–1684.

[2] M. Fink, "Time-reversed acoustics," *Scientific American*, pp. 91–97, Nov. 1999.

[3] L. C. V. Atta, "Electromagnetic reflector," U.S. Patent 2,908,002, 1959.

[4] C. Y. Pon, "Retrodirective array using the heterodyne technique," *IEEE Trans. Antennas Propag.*, vol. 12, no. 2, pp. 176–180, Mar. 1964.

[5] G. S. Shiroma, R. Y. Miyamoto, and W. A. Shiroma, "A full-duplex dual-frequency self-steering array using phase detection and phase shifting," *IEEE Trans. Microw. Theory Tech.*, vol. 54, no. 1, pp. 128–134, Jan. 2006.

[6] A. Zamora, M. K. Watanabe, T. F. Chun, J. M. Akagi, and W. Shiroma, "An inter-element phase-detecting retrodirective array for nonuniform wavefronts," in *IEEE MTT-S Intl. Microwave Symposium Dig.*, Boston, MA, Jun. 2009, pp. 817–820.

[7] M. K. Watanabe, R. N. Pang, B. O. Takase, J. M. Akagi, G. S. Shiroma, and W. A. Shi-

roma, "A 2-D phase-detecting/heterodyne-scanning retrodirective array," *IEEE Trans. Microw. Theory Tech.*, vol. 55, no. 12, pp. 2856–2864, Dec. 2007.

[8] J. M. Akagi, A. Zamora, M. K. Watanabe, and W. A. Shiroma, "A self-steering array using power detection and phase shifting," in *IEEE MTT-S Int. Microwave Symp. Dig.*, Atlanta, GA, Jun. 2008, pp. 1325–1328.

[9] B. O. Takase, M. K. Watanabe, R. N. Pang, J. M. Akagi, G. S. Shiroma, and W. A. Shiroma, "Analysis of phase-conjugating arrays in multipath environments," *IEEE Trans. Microw. Theory Tech.*, vol. 57, no. 3, pp. 524–530, Mar. 2009.

[10] P. V. Brennan, "Investigation into the multipath performance of self-phased arrays," *IEE Proceedings*, vol. 136, no. 1, pp. 47–52, Feb. 1989.

[11] J. Tuovinen, G. Shiroma, W. Forsyth, and W. Shiroma, "Multipath communications using a phase-conjugate array," in *IEEE MTT-S Intl. Microwave Symposium Dig.*, Philadelphia, PA, Jun. 2003, pp. 1681–1684.

[12] N. Buchanan and V. Fusco, "Bit error rate performance enhancement of a retrodirective array over a conventional fixed beam array in a dynamic multipath environment," *IEEE Trans. Microw. Theory Tech.*, vol. 58, no. 4, pp. 757–763, Apr. 2010.

[13] C. Loadman and Z. Chen, "A study of retrodirective array performance in the presence of multipath," in *Proc. of the* 2^{nd} *Annual Conference on Communication Networks and Services*, May 2004, pp. 56–60.

[14] T. F. Chun, M. K. Watanabe, A. Zamora, J. M. Akagi, and W. Shiroma, "Multiple in-

terrogation of phase-conjugating arrays," in *IEEE MTT-S Intl. Microwave Symposium Dig.*, Boston, MA, Jun. 2009, pp. 1193–1196.

[15] T. F. Chun, M. K. Watanabe, A. Zamora, R. T. Iwami, J. M. Akagi, and W. Shiroma, "Analysis of phase-conjugating arrays in multiple-interrogator environments," in *IEEE International Conference on Wireless Information Technology and Systems*, Honolulu, HI, Aug. 2010.

[16] R. Y. Miyamoto, G. S. Shiroma, and W. A. Shiroma, "A high-directivity transponder using self-steering arrays," in *IEEE MTT-S Intl. Microwave Symposium Dig.*, Fort Worth, TX, Jun. 2004, pp. 1683–1686.

[17] G. S. Shiroma, R. Y. Miyamoto, J. D. Roque, J. M. Cardenas, and W. A. Shiroma, "A high-directivity combined self-beam/null-steering array for secure point-to-point communications," *IEEE Trans. Microw. Theory Tech.*, vol. 55, no. 5, pp. 838–844, May 2007.

[18] D. Goshi, K. M. K. H. Leong, and T. Itoh, "Interleaved retrodirective sub-arrays for null-steering interference rejection," in *IEEE MTT-S Intl. Microwave Symposium Dig.*, Honolulu, HI, Jun. 2007, pp. 1719–1722.

[19] R. L. Haupt, "Phase-only adaptive nulling with a genetic algorithm," *IEEE Trans. Antennas Propag.*, vol. 46, no. 6, pp. 1009–1015, Jun. 1997.

[20] C. A. Balanis, *Antenna Theory.* New Jersey: John Wiley & Sons, Inc., 2005.

[21] W. E. Forsyth and W. A. Shiroma, "A retrodirective antenna array using a spatially

fed local oscillator," *IEEE Trans. Antennas Propag.*, vol. 50, no. 5, pp. 638–640, May 2002.

[22] J. Huang and J. Encinar, *Reflectarray Antennas*. New Jersey: John Wiley & Sons, Inc., 2008.

[23] S. Hum and M. Okoniewski, "An electronically tunable reflectarray using varactor-diode tuned elements," in *IEEE AP-S/URSI Symposium*, Monterey, CA, Jun. 2004, pp. 1325–1328.

[24] A. M. S. Bildik, C. Fritzsch and R. Jakoby, "Tunable liquid crystal reflectrray with rectangular elements," in *German Microwave Conference*, 2010, Conf. Pub. 461, pp. 1–4,15–17.

[25] J. F. R. Marin, A. Mossinger and R. Jakoby, "Characterization of 35 ghz tunable reflectarray unit-cells using highly anisotropic liquid crystal," in *German Microwave Conference*, March 2010, Karlsruhe, Germany.

[26] S. A. Long and G. H. Huff, "Experiments on a fluidic loading mechanism for beam-steering reflectarrays," in *IEEE International Conference on Wireless Information Technology and Systems*, Honolulu, HI, Aug. 2010.

[27] F. Mugele and J. C. Baret, "Electrowetting: from basics to applications," *J. Phys.: Condens. Matter*, vol. 17, pp. R705–R744, 2001.